

Anonymous Referee #1

General comments and recommendation

This study looks at trends in aerosol optical thickness (AOT) from MODIS and MISR, as well as trends in aerosol shortwave direct radiative effect (DRE) from CERES data. CALIOP data are also used. This is in part an update of earlier work by some of the authors, updated using newer versions of the MODIS data, and in part a new analysis. The study is within scope of ACP and the methodology is fairly standard and reasonable. The topic is of relevance and interest.

I did however find it a bit hard to read. Some sections are quite verbose and hard to pick out the key take-away messages. This is however in part the authors being thorough in comparing this analysis to their previous MODIS analysis, as well as in noting some limitations of one of the CERES data products. So it's hard to give advice on how to remedy this while keeping the analysis thorough (which is an aspect I definitely like). As a result I recommend publication after minor revisions, listed below, mostly to address writing style. There is however also one important statistical error in terms of discontinuous trends in Figure 11 which needs to be addressed to make the manuscript technically correct.

Response: We thank the reviewer for his/her constructive suggestions and comments. We tried to re-organize the paper as suggested and details are shown below. Also, we have also modified Figure 11 as suggested, to include piecewise linear regressions as suggested.

Specific comments:

Title: MISR should be added here. Maybe CALIOP too? Or the authors could remove the specific sensor names and say "various satellite products" or something.

Title: "Longer term variation" is a bit clunky and, to me at least, implies longer than single-sensor records (which isn't what is discussed in this study). I guess the authors chose this wording to make a contrast with their previous studies, which were decadal? Perhaps "21st century variations" would be better, since the data start in 2000 or later?

Response: These are nice suggestions. We have revised the title to:
A Study of 15-Year Aerosol Optical Thickness and Direct Shortwave Aerosol Radiative Effect Trends Using MODIS, MISR, CALIOP and CERES

Lines 103-104: a reference for MISR should be added here. I'm not sure what the best one is. Perhaps Kahn et al (JGR, 2010), which I think is the main validation study for this version of the data?

Response: Kahn et al., 2010 has been added to the reference list.

Line 109: As a minor point, the MODIS product doesn't do "spectral AOT retrievals". It retrieves AOT at 550 nm and the weighting between fine and coarse aerosol modes, for various mode combinations. Spectral AOT is derived from these parameters. I suggest something like "provides spectral AOT at seven wave lengths" or even just removing the bit about wavelengths, since only 550 nm (the main data product) is used in this study anyway.

Response: Done. We have changed the sentence to "provides spectral AOT at seven wave lengths" as suggested.

Line 110: "increased resolution" isn't quite right here, since the data are coarser at the edge of the swath. I think the authors either mean "increased pixel size" or "decreased resolution".

Response: Thanks for the suggestion. We have changed to "increase pixel size" as suggested.

Line 160: This line says only data with CP > 95% are used, while line 182 says CP > 99% are used. Is this inconsistent or am I misunderstanding something here? If these are for two different parts of the analysis, why the different thresholds?

Response: The first threshold (CP > 95%) is used for the initial collocation step. This would allow us to perform a sensitivity study to evaluate the impact of cloud fraction on the analysis as shown in Table 5. Only collocated pairs with CP > 99% are used in the final analysis. We have revised the sentence as follows to avoid confusion.

"Note that only CERES pixels that have a MODIS reported cloud fraction of 1% or less are used in the final process. A more relaxed CP threshold of 95% is adopted here, partially for studying the impact of cloud contamination on CERES derived SWAREs as shown in Table 5"

Lines 167-169: I'm not sure why the first part of this sentence is needed. I think it's fine just to say the arithmetic mean MODIS AOT is used.

Response: We have made the change as suggested. Thanks.

Line 186: There have been a large number of studies into cirrus contamination of MODIS AOT data, not just Toth et al (2013), and many were well before that paper. I suggest rewording this to make it clearer that was not the first study, and maybe cite some of those other ones too.

Response: Thanks for your suggestion. We have revised the sentence as "Several studies have suggested that MODIS AOT retrievals may be contaminated with optically thin cirrus clouds (OTC, e.g. Kaufman et al., 2005, Huang et al., 2011, Feng et al., 2011, Toth et al., 2013)."

We have added the papers to the reference list.

Kaufman, Y. J., Remer, L.A., Tanre, D., Li, R.-R., Kleidman, R., Mattoo, S., Levy, R., Eck, T., Holben, B.N., Ichoku, C., Martins, V., and Koren, I.: A critical examination of the

residual cloud contamination and diurnal sampling effects on MODIS estimates of aerosol over ocean, IEEE Trans. Geosci. Remote Sens., 43, 2886–2897, 2005.

Huang, J., Hsu, N.C., Tsay, S.C., Jeong, M.-Y., Holben, B.N., Berkoff, T.A., and Ellsworth, J.W.: Susceptibility of aerosol optical thickness retrievals to thin cirrus contamination during the BASE-ASIA campaign, J. Geophys. Res. 116, D08214, doi:10.1029/2010JD014910, 2011.

Feng, Q., Hsu, N.C., Yang, P., and Tsay, S.-C.: Effect of thin cirrus cloud on dust optical depth retrievals from MODIS observations, IEEE Tran. Geosci, Remote Sens., 49, No.8, 2011.

Lines 200-207: This paragraph doesn't really fit in this Section, which is otherwise describing the data sets used. I think it should be broken out into a new section summarising how trends are calculated and assessed (i.e. construction of time series of monthly deseasonalized AOT anomalies). It would be useful to add a bit of brief information about these two significance methods here as well. For example the Weatherhead approach attempts to account for autocorrelation, which is important in some areas for monthly AOT time series.

Response: As suggested, we have moved this paragraph to a later section and added additional discussions.

Section 3.1: I think I understand what was done here but from the discussion and tables it isn't always clear what results apply to what bit. My understanding is the authors (1) compare C5 trends to C6 trends (for 2000-2009) and (2) compare C5 trends to the Zhang and Reid (2010) trends, which used a 'data assimilation (DA) grade' version of the MODIS products. So in this way they assess whether differences are more because of the C5/C6 change or the fact that Zhang and Reid (2010) used the DA-grade product and there isn't a C6 equivalent (that I know of) DA-grade product. To help with this I suggest restructuring this section as follows:

1. Move the bit about how trends are calculated to a new section earlier in the paper (see prior comment about lines 200-207). This will help streamline the text by putting the methodology in a methodology section.

Response: Done. Thanks for the suggestion.

2. Remove the text defining regions from the main body, since regions are already defined in Table 2, where they're easier to read.

Response: Done.

3. Split out the analysis into two separate subsections, one to compare C5 vs. C6 trends for the 2000-2009 period, the other to compare C5 trends with and without the DA process. (Alternatively, since the conclusion seems to be that the differences are mostly minor, you could

put in a few sentences that you looked at it but didn't find that things had changed much, and then just cut out the rest of the section.)

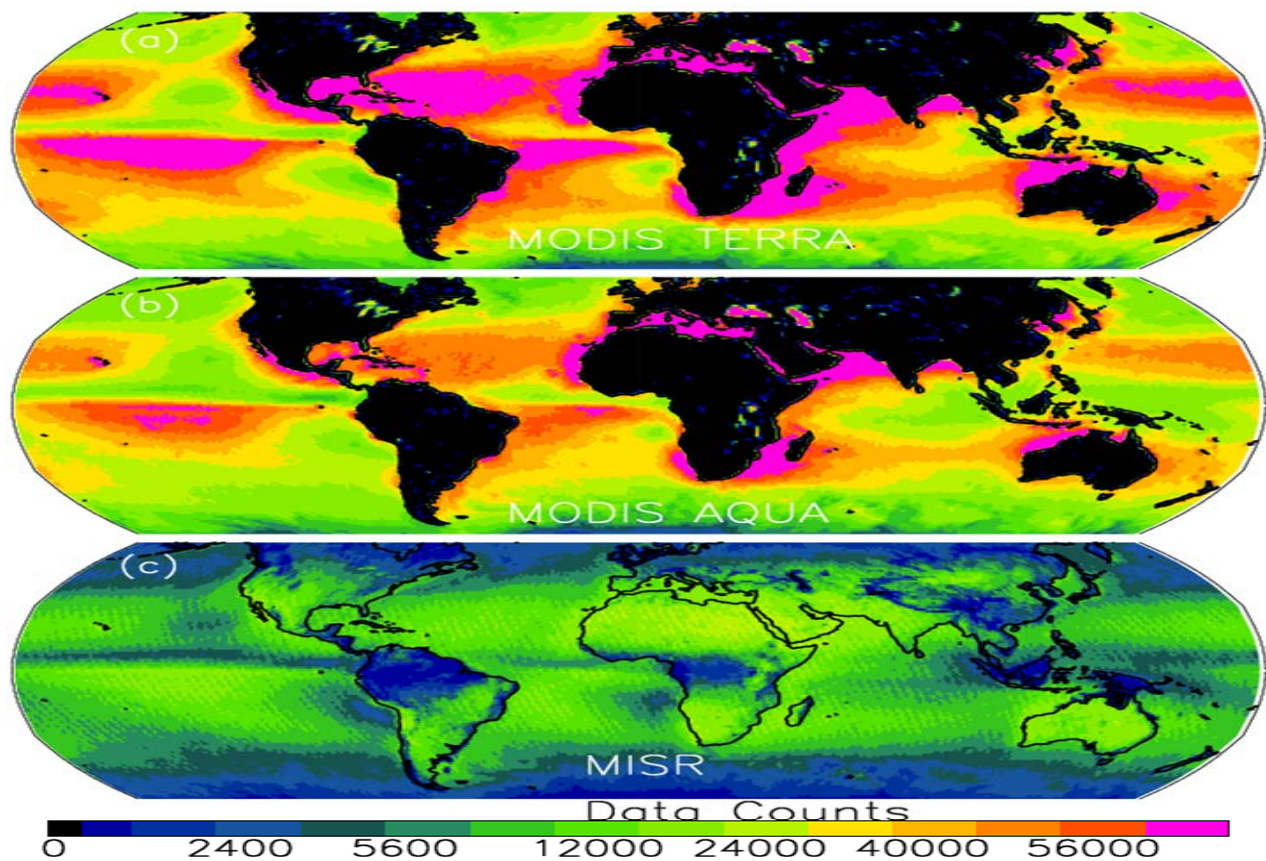
Response: Note that DA data are not used in this study and the comparison of C5 MODIS and DA datasets has already been reported by Zhang and Reid, 2010. To avoid confusion, we have revised the following paragraph:

“Here regional and global mean C5 AOTs are derived using similar steps as were used in constructing the C6 AOT data, which are differ from the data-assimilation quality C5 MODIS DT data as used in Zhang and Reid (2010). Still, as suggested from Zhang and Reid (2010), although QA steps could lower the mean global over ocean AOTs from ~0.15 to ~0.11, in part due to the removal of cloud contaminated retrievals, minor impacts on the AOT trend analysis are reported.”

Line 273: I guess the authors use 1000 data counts because the MODIS level 3 aerosol products don't provide a count of number of days per month, despite various requests over the years. It would be good to indicate briefly the main areas where this removes data, and what the typical variations of data volume are in other grid cells (e.g. are the results sensitive to the threshold choice, or do most grid cells have many times more than 1000 retrievals?). From Figure 2 it appears that for MODIS it doesn't remove (m)any ocean grid cells in the studied latitude range. For MISR the gaps are roughly where I'd expect from e.g. cloud patterns in the tropics.

Response: The data count is rather an arbitrary number used to remove some over land water retrievals over scenes such as lakes. This is also partially used to ensure sufficient data are included in the trend analysis. Attached below is the data count plot associated with Figure 2. This plot is not included in the paper, as the paper is already very long. We have added the following sentence to clarify the concern:

“(this is an arbitrary threshold selected for removing some over land water retrievals over scenes such as lakes. It is also partially used for ensuring sufficient data are included in the trend analysis)”



Line 275: Remer et al (2006) was before the MODIS Collection 5 release was complete, and you are using Collection 6 data. I don't know of a similar study to Remer et al (2006) using Collection 6 data, so it's probably still fine to cite that study here, but may be worth noting that was for an older data product version.

Response: Done. We have added the following discussion as suggested: "Remer et al. (2006) using 3 years of C5 MODIS data"

Lines 282-285: are these area weighted or simple mean? This should be stated. 1 degree grid cells at high latitudes are a lot smaller in real terms than those at the Equator. It may not affect the offset and trends shown in the figure too much, but may affect the baseline global-average AOT, since AOT tends to be higher in the Equatorial belt due to continental outflow.

Response: Area weighting is not applied and arithmetic averages are applied to compute means. We have added "simple arithmetic mean" into the text as suggested.

Lines 300-316: This is an interesting and I think pretty reasonable way of addressing/correcting for potential calibration drift, so that's good that the authors have done so. The basic idea is that

if there's a trend in a region that's expected to be stable, one can subtract that trend from apparent trends elsewhere. However a caveat here is that assumes that the calibration degradation propagates linearly into AOT. That is probably fine for areas with AOT close to that of the remote region used as a baseline. But for example a 3% change in reflectance may cause a certain change in AOT when the true AOT=0.1 as compared to at e.g. AOT=0.5, since the radiative transfer isn't linear in AOT. The correction might therefore be an under/over-correction in those higher-AOT areas. Again, there's probably no simple better way of approaching this so the method is reasonable to use here. But since many readers of the article might not be familiar with the underlying radiative transfer and retrieval algorithms, I think this caveat should be mentioned.

Response: Thanks for the suggestion. We have added the following paragraph as suggested: “A caveat here is that we assume that the calibration degradation propagates linearly into AOT. The correction might therefore be an under/over-correction in those higher-AOT areas.”

Lines 339-340: the authors state that “the rates of increase of aerosol loading have slowed down over the last five years” because trend estimates over the period 2000-2015 are less positive than those for 2000-2009. That is certainly one possibility, but the statement is unsupported by the evidence. The trends for both periods may be statistically distinct from zero, but are they statistically different from each other? That is the relevant factor here. Only if so can one say that that the trend has slowed. The reader can't tell if this is the case, since uncertainty estimates for the trends are not shown. I suggest the authors look into this and either add text supporting it (if the trends are statistically distinguishable from each other) or remove this text (if they're not).

Response: We are unclear about the comments. For trends estimated for the periods of 2000-2009 and 2000-2015, data that are used for estimating trends are the same for the first ten years (2000-2009). Thus the trend changes by adding 5 more years of data are likely linked to new data added to the analysis. The flattening of the last 5 years of trends for the Bay of Bengal and Arabian Sea can also be seen from Figure 4. We revised the sentence as below to avoid confusion:

“However, the rates of increase of aerosol loading have plausibly slowed down over the last five years for both regions, indicated by ~20-30% reductions in AOT trends when estimated using the near full Terra data records. Flattening of AOT trends with respect to time can also be observed in Fig. 4 for both regions for 2010-2015.

Sections 3.2, 4: As a general comment related to the above, it would be good if the estimates of trend precision could be given in the text when specific numbers are mentioned. For example on line 428 the SWARE trends in a region are given as 39.8 and 43.7 W/m²/AOT for Aqua and Terra. Without uncertainty estimates on those numbers, we don't know if the 4 W/m²/AOT difference between the two sensors is significant or within the uncertainty of the data sets used. This is just one example, the comment extends throughout the paper. It doesn't necessarily need to be given for every statistic in the paper but when it is a key result or comparison between two quantities, it makes sense to consider the uncertainty estimates. I realise that often both WH and MK methods are used to estimate significance in this study; it probably doesn't matter too much

which method is used when you're quoting these uncertainties for the above points (as I'm guessing they will be similar).

Response: Trend uncertainty analysis has been included in section 4.2. Trend significances are also discussed with the use of the WH and MK methods. The numbers referred from this comment are aerosol SW direct forcing efficiencies, not trends. To estimate the uncertainties in aerosol SW direct forcing efficiencies, in situ observations may be needed, and the evaluation process can be a paper of its own. Thus, we leave this topic for a future paper.

Section 5: This section says it compares results to other trend studies, but really it only compares results to other trend studies published by the same authors. There are a number of other regional/global trend analyses using satellite aerosol data which could be considered. For example various Mischenko group papers for AVHRR over ocean, Thomas (ACP 2010) for ATSR over ocean, Hsu (ACP 2012) for SeaWiFS land and ocean, Yoon (ACP 2011) for SeaWiFS regionally, Yoon (AMT 2012) for AERONET, Dey and Girolamo (JGR 2011) for MISR in India, Babu (JGR 2013) for Indian surface observations. It would be good to include some of these more independent studies in the discussion here. The point is there's a lot of work which has been done and is relevant to the discussion here but isn't acknowledged. Maybe there isn't space to include anything but the authors only self-citing here is a bit of a let down.

Response: In fact, we have tried to compare region trends from other studies but only realized that each study has its own domain defined differently, making the inter-comparison less intuitive, as sampling differences also need to be considered. Thus, we only selected studies that report trends with similar geographic domains.

Figures 6, 7: I couldn't find a mention of how the black lines in panels a, c here were calculated. This should be added. Also, it seems like results like this are the basis for quoting an aerosol forcing efficiency in units of $W/m^2/AOT$. From the shape of these curves it looks a bit more like a logarithmic fit with a kink around $AOT=0.15$. I know people like to think in units of $W/m^2/AOT$ but perhaps this paper is a good place to point out that the relationships aren't really that linear. This is something which could be highlighted again in the Conclusions (either in list items 5, 6, or a new item).

Response: The black lines are global means. We have added a line in the figure caption to clarify this:

“Color lines are for selected regions and the black thick line is for global oceans.”

Also, based on the figure, aerosol forcing efficiency is a non-linear function of AOT. We have added discussions as suggested in the text:

“Figure 6b shows the Aqua MODIS AOT and Aqua SW_{ssf} relationship (non-linear) for 5 selected regions”

“It also worth noting that a non-linear relationship is found between SW_{ARE} and AOT.”

Figure 11 and associated text: This bit needs further work. It is fine to show trends split by periods, but the discontinuity at the breakpoint is not physical; it implies a sudden jump in the system. Having a breakpoint discontinuity is a sign that the derived values are not robust. There are methods to identify breakpoints in trends, and fit a piecewise continuous trend, rather than an unphysical broken trend. (I think the Weatherhead paper mentioned may discuss this? If not then some of her other work.) The authors should repeat this part of the analysis using a continuous piecewise fit. It's quite possible that this may affect the conclusions. Even if you get a similar answer, it will be on firmer theoretical ground, so it is necessary to do otherwise the manuscript contains methodological errors.

Response: We have implemented a method as mentioned in Tomé and Miranda (2004) to detect the breakpoints and details of the approaches have been included in Zhang et al. (2017).

We have added the following discussions in the text as well:

“Here a piecewise linear fit method from Tomé and Miranda (2004) is applied to detect turning points in trends, similar to what is suggested by Zhang et al. (2017). Also, similar to Zhang et al. (2017), we assume a minimum of 36 months between any two detected turning points.”

Anonymous Referee #2

General comments and recommendation

This study computes AOT and SWARE trends from multiple satellite instruments. Although no particular issues are present in the methodologies used in the study, the manuscript would benefit from a more focused presentation. The motivations for this work isn't clearly stated and it is also not clear how this work is distinct from the authors' previous papers. Relative to the authors' previous work, this study uses additional datasets, a longer time period and updates to C6 of the MODIS data products. Given this study is essentially a repeat of previous work, I would encourage to authors to spend less time comparing every detail between this and their previous work and instead concisely present to the reader what new knowledge this study gives compared to the group's previous work. While bits and pieces of this are found throughout the paper, they are difficult to pick out in the long-winded presentation.

Response: We thank the reviewer for his/her constructive comments.

As the reviewer mentioned, in Zhang and Reid, 2010, 10-year AOT trends (2000-2010) were estimated, using C5 MODIS DT and MISR aerosol products with a focus on 10 selected regions. With the release of C6 MODIS DT products that have non-trivial changes in the retrieval process, and with the availability of a dataset with a longer study period (2000-2015), there is a need to understand the changes in AOT trends due to the above mentioned changes. In fact, we have reported a slowdown in positive AOD trends over Bay of Bengal, Arabian Sea and China. In addition, we found significant positive trends for the Red Sea and Persian Gulf regions (new regions that are not included in Zhang and Reid, 2010). Those findings warrant reporting. We have modified some discussions, as well as reorganized some sections, also per suggestions from reviewer 1 (see responses to reviewer 1 for details). Still, we felt the remaining discussions are needed to help readers who are not familiar with Zhang and Reid, 2010. Also, the reviewer notes that there is simply an "addition of new datasets." However the use of CERES fluxes is major undertaking, and it is important to show how AOD based and CERES based trends compare. Indeed, the suspected calibration drift in CERES reported in this paper sets a baseline as to how much "flux" can be compared to AOD based estimates.

Additionally, there many other studies of AOT trends outside the authors' previous work that are not cited in the manuscript which require recognition. The addition of the SWARE analysis is diminished somewhat since, in the context of the radiation budget, trends in instantaneous fluxes isn't particularly useful. Additional, although the authors appear to be surprised by this, the SWARE is largely controlled by AOT, so it is expected that trends will be highly correlated. This make the SWARE analysis somewhat redundant. Concerning the overall motivation for this study: given the large uncertainties, how do these trends help our understanding of aerosols and their role in the climate system?

Response: Firstly, as suggested, we have cited more papers as listed below:

Chin, M., Diehl, T., Tan, Q., Prospero, J. M., Kahn, R. A., Remer, L. A., Yu, H., Sayer, A. M.,
Bian, H., Geogdzhayev, I. V., Holben, B. N., Howell, S. G., Huebert, B. J., Hsu, N. C.,

- Kim, D., Kucsera, T. L., Levy, R. C., Mishchenko, M. I., Pan, X., Quinn, P. K., Schuster, G. L., Streets, D. G., Strode, S. A., Torres, O., and Zhao, X.-P.: Multi-decadal aerosol variations from 1980 to 2009: a perspective from observations and a global model, *Atmos. Chem. Phys.*, 14, 3657–3690, <https://doi.org/10.5194/acp-14-3657-2014>, 2014.
- Mishchenko, M. I., Liu, L., Geogdzhayev, I. V., Li, J., Carlson, B. E., Lacis, A. A., Cairns, B., and Travis, L. D.: Aerosol retrievals from channel-1 and -2 AVHRR radiances: Long-term trends updated and revisited, *J. Quant. Spectrosc. Ra.*, 113, 1974–1980, 2012.
- Thomas, G. E., Poulsen, C. A., Siddans, R., Sayer, A. M., Carboni, E., Marsh, S. H., Dean, S. M., Grainger, R. G., and Lawrence, B. N.: Validation of the GRAPE single view aerosol retrieval for ATSR-2 and insights into the long term global AOD trend over the ocean, *Atmos. Chem. Phys.*, 10, 4849–4866, doi:10.5194/acp-10-4849-2010, 2010.
- Zhao, X.-P., Chan, P. K., and Heidinger, A. K.: A global survey of the effect of cloud contamination on the aerosol optical thickness and its long-term trend derived from operational AVHRR satellite observations, *J. Geophys. Res.*, 118, 2849–2857, doi:10.1002/jgrd.50278, 2013.

We understand the existence of uncertainties in this study, but this is the first time SWARE trends have been evaluated with the use of space-borne observations alone. As suggested from Figs. 6 and 7, SWARE is a function of both AOD and aerosol type. Different aerosol species could have drastically different aerosol SW forcing efficiencies. And as the first reviewer suggested, the relationship between SWARF and AOD is rather non-linear as well. Thus, in traditional approaches for aerosol forcing studies (either models or radiative transfer calculations), detailed information about the temporal and spatial variations of aerosol properties are needed. An innovative approach is applied in this study, to directly estimate SWARE and SWARE trends from the collocated MODIS and CERES data, which doesn't not require a-priori knowledge of aerosol speciation. Thus, the results from this study can be used to inter-compare with model/radiative transfer model based SWARE analyses for evaluation and validation as well as for further estimating anthropogenic aerosol SWARE trends (e.g. Sundar et al., 2005).

Christopher, S. A., J. Zhang, Y. J. Kaufman, and L. A. Remer (2006), Satellite-based assessment of top of atmosphere anthropogenic aerosol radiative forcing over cloud-free oceans, *Geophys. Res. Lett.*, 33, L15816, doi:[10.1029/2005GL025535](https://doi.org/10.1029/2005GL025535).

In the conclusion the authors state that "This study suggests that comprehensive observational systems can and should be used in future studies to gain a better understanding of any changes in atmospheric aerosol states." But what specific understanding have we gained with this study beyond a set of descriptive statistics? Given the large uncertainties, these trends are far from being climate monitoring quality, how does that limit the impact of work like this? Do we observations with lower uncertainties or is getting a few robust regional trends good enough? Given the large calibration drifts, should the goal be to develop of more advanced drift removal method than using the Remote Ocean region? More discussion on these sort of question and the broader implications of this work is needed in the introduction/conclusion.

Response: In this study, we compared aerosol trends from both passive and active-based methods (MODIS, MISR, CALIOP), over both cloud free and above cloud studies, as well as with both narrowband and broadband observations. Note that different instruments have different

sampling methods with different uncertainties under different observing conditions. Also, observations from active-based sensors can be used for reporting aerosol trends at both vertical and horizontal domains. While the above clouds aerosol studies evaluate aerosol trends from only the atmospheric columns above clouds. The broadband analysis covers the whole solar spectrum. We believe it is worth reporting the consistencies and inconsistencies we found for studies with different observing methods and with different instruments thus setting an observational baseline. We have added the following discussion in the conclusion section and revised the conclusion section.

“Note that the above mentioned studies are derived with different instruments that have different sampling methods with different uncertainties under different observing conditions. The fact that consistencies are found from those studies, adds fidelity to some of the studies that are difficult to evaluate otherwise.”

Also, to avoid confusion, we removed the following discussion:

“This study suggests that comprehensive observational systems can and should be used in future studies to gain a better understanding of any changes in atmospheric aerosol states.”

What is the point of keeping the seasonal cycle in some of the plots, but not others? Unless there is some particular reason for this, I would find it more instructive if all comparisons were deseasonalized.

Response: The monthly and seasonal averages of AOT and SWARE, Figs. 3a and 8a, respectively, are shown in order to illustrate the global AOD and SWARE values as well as for visual comparison to the deseasonalized time series. Due to the fact that the all-sky flux trends are not analyzed in further detail, Fig. 9 is also not deseasonalized.

The color bars on Figs. 1 and 12 make it difficult to infer any quantitative information. I suggest that the max/min range and the near-zero white portion be narrowed.

Response: We have revised the color bars as suggested as shown below. However, we still prefer to keep the original color bars to highlight significant signals in the paper, and thus no change is made to the paper.

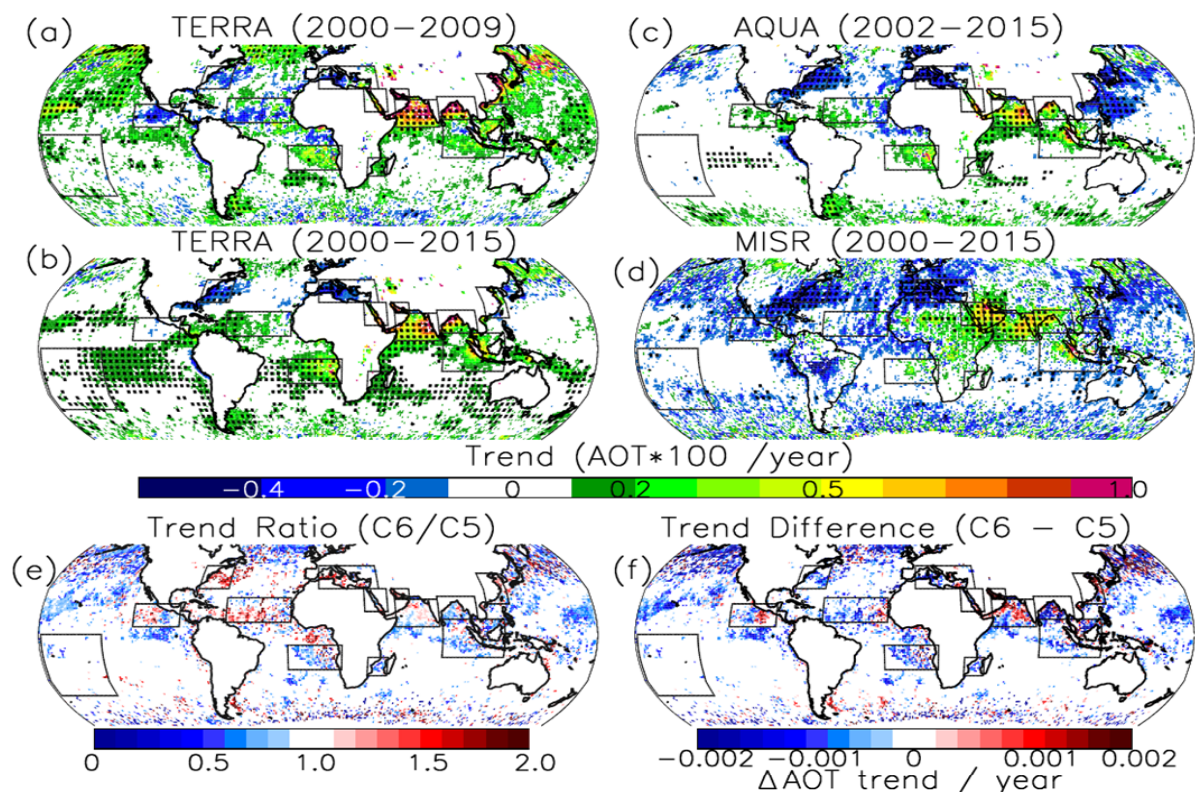


Figure 1. Spatial distribution of trends for (a) over ocean 942 Terra MODIS DT AOT for 2000-2009, (b) over ocean Terra MODIS DT AOT for 2000-2015, (c) over ocean Aqua MODIS DT AOT for 2002-2015 and (d) over land and ocean Terra MISR AOT for 2000-2015 for every $1^\circ \times 1^\circ$ bin. (e) Ratios of MODIS C6 to C5 AOT trends for the study period of 2000-2009, and (f) Differences in MODIS C6 to C5 AOT trends for the study period of 2000-2009. Regions with statistically significant trends at a confidence interval of 95% are highlighted with black dots. Figs. 1e and 1f are constructed with the use of grids with AOT trends above or below ± 0.0001 AOT/year.

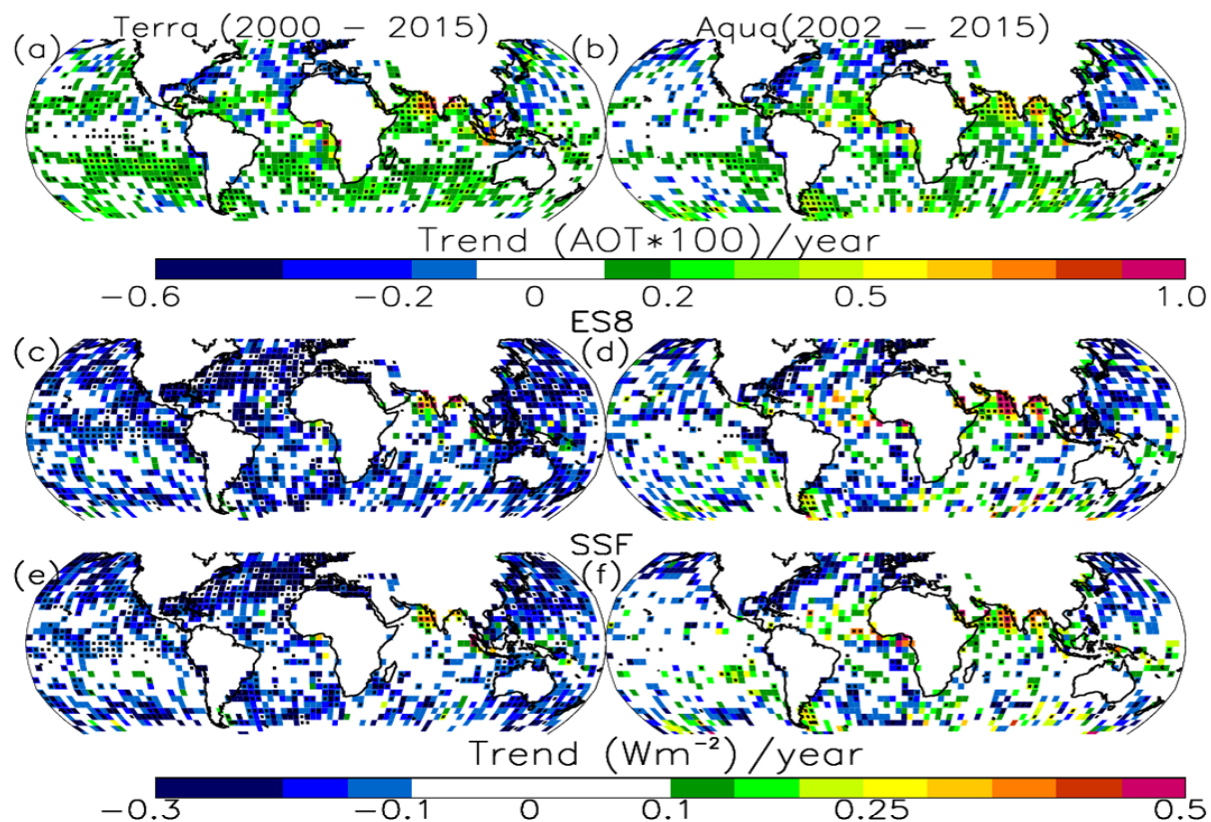


Figure 12. Spatial distribution of gridded AOT trends for (a) 16 year Terra (2000-2015) and (b) 14 year Aqua (2002-2015) for every $4 \times 4^\circ$ (Latitude/Longitude) bin derived from the collocated MODIS-CERES dataset. AOT trends are constructed using seasonally-averaged AOTs. (c) Spatial distribution of cloud-free-sky CERES ES-8 SW flux trends estimated using the collocated Terra MODIS-CERES data for the study period of 2000-2015. (d) Similar to Figure 12c, but using the collocated Aqua MODIS-CERES (ES-8) dataset for the study period of 2002-2015. (e-f) Similar to Figs. 12c and 12d, but for using CERES SSF data. Grids with statistically significant AOT/clear-sky SW flux trends at the 95 % confidence interval are shown in black dots.

Why is Eq (1) is opposite the usual sign convention?

Response: The definition of short wave aerosol radiative forcing (SWARF) is the difference in cloud-free sky short wave flux (SW) observed without (F_{clear}) and with (F_{aero}) the presence of aerosol. It is typically used in the satellite based SWARE studies.

Lines 54-55: what is meant by "detecting aerosol plumes". MODIS doesn't have an aerosol mask.

Response: We have changed "detecting aerosol plumes" to "reporting finer scale aerosol optical properties" in the text.

Lines 60-62: Remove this sentence. The Terra/Aqua time series is not long enough to directly observe climate forcing. Additionally, the authors don't examine the SW direct forcing (i.e. radiative effect of only anthropogenic aerosols).

Response: Done.

What version of the CERES data products are being used?

Response: Edition 3A for SSF and Edition 3 for ES8. We have added that to the text.

Lines 147-148: not sure what is meant by this line. What else could aerosol be classified as

Response: The CERES ES8 data set contains no information about aerosols. We have revised the sentence to:

“No aerosol properties are considered in constructing ERBE ADMs”

line 175: change "Overland" to "Over land"

Response: Done.

line 186: remove "even"

Response: Done. We have revised the sentence to “Several studies have suggested that MODIS AOT retrievals may be contaminated with optically thin cirrus clouds (OTC, e.g. Kaufman et al., 2005, Huang et al., 2011, Feng et al., 2011, Toth et al., 2013).:”

lines 194-197: why is the C3M data mentioned if its never going to be used?

Response: Some readers may be familiar with the C3M products. We want to be clear on why we didn't use the C3M data.

lines 197-199: remove this sentence

Response: We prefer to keep the sentence to remind some readers of the reason that C3M data are not used.

Line 215: remove "trend paper"

Response: Done.

Line 240/251: remove "For illustrative purposes"

Response: Done.

Lines 273-274: remove "A quick comparison"

Done.

Line 293: remove interestingly.

Response: Done

line 492: remove "Surprisingly"

Response: Done.

~~A Study of the Longer Term Variation of Aerosol Optical Thickness and Direct Shortwave Aerosol Radiative Effect Trends Using MODIS and CERES~~
A Study of 15-Year Aerosol Optical Thickness and Direct Shortwave Aerosol Radiative Effect Trends Using MODIS, MISR, CALIOP and CERES

Formatted: Font: 14 pt

Ricardo Alfaro-Contreras¹, Jianglong Zhang¹, Jeffrey S. Reid², and Sundar Christopher³

¹Department of Atmospheric Sciences, University of North Dakota, Grand Forks, ND

²Marine Meteorology Division, Naval Research Laboratory, Monterey, CA

³Department of Atmospheric Science, The University of Alabama in Huntsville

Submitted to Atmospheric Chemistry and Physics
(2017)

Corresponding Author: jzhang@atmos.und.edu

21 Abstract

22 By combining Collection 6 Moderate Resolution and Imaging Spectroradiometer (MODIS)
23 and Version 22 Multi-angle Imaging Spectroradiometer (MISR) aerosol products with Cloud and
24 Earth's Radiant Energy System (CERES) flux products, the aerosol optical thickness (AOT, at
25 $0.55\mu\text{m}$) and Short-Wave Aerosol Radiative Effect (SWARE) trends are studied over ocean for
26 the near full Terra (2000-2015) and Aqua (2002-2015) data records. Despite differences in
27 sampling methods, regional SWARE and AOT trends are highly correlated with one another.
28 Over global oceans, weak SWARE (cloud free SW flux) and AOT trends of $0.5 - 0.6 \text{ Wm}^{-2}$ (-0.5
29 $\text{to } -0.6 \text{ Wm}^{-2}$) and $0.002 \text{ AOT decade}^{-1}$ were found using Terra data. Near zero AOT and
30 SWARE trends are also found for using Aqua data, regardless of Angular Distribution Models
31 (ADMs) used. Regionally, positive SWARE and AOT trends are found over the Bay of Bengal,
32 Arabian Sea, Arabian/Persian Gulf and the Red Sea, while statistically significant negative trends
33 are derived over the Mediterranean Sea and the eastern US coast. In addition, the global mean
34 instantaneous SW aerosol direct forcing efficiencies are found to be $\sim -60 \text{ Wm}^{-2}$ per AOT, with
35 corresponding SWARE values of $\sim -7 \text{ Wm}^{-2}$ from both Aqua and Terra data, and again,
36 regardless of CERES ADMs used. Regionally, SW aerosol direct forcing efficiency values of \sim
37 -40 Wm^{-2} per AOT are found over the southwest coast of Africa where smoke aerosol particles
38 dominate in summer. Larger (in magnitude) SW aerosol direct forcing efficiency values of -50
39 $\text{to } -80 \text{ Wm}^{-2}$ per AOT are found over several other dust and pollutant aerosol dominated regions.
40 Lastly, the AOT and SWARE trends from this study are also inter-compared with aerosol trends
41 (such as active-based) from several previous studies. Findings suggest that a cohesive
42 understanding of the changing aerosol skies can be achieved through the analysis of observations
43 from both passive- and active-based analyses, as well as at both narrow-band and broad-band
44 data sets.

1. Introduction

The significance of aerosol particles on global and regional climate variations has been extensively studied for the past two decades with both observational- and modeling-based approaches (IPCC, 2013). In particular, studies have suggested that the direct shortwave (SW) Aerosol Radiative Effect (SWARE), which refers to the impacts of aerosol particles on Earth's radiation balance through the absorption and scattering of incoming SW solar energy, can be estimated with the combined use of broadband and narrowband observations at the shortwave spectrum (e.g. Zhang et al., 2005a;b; Loeb and Kato, 2002). For example, using one year of collocated Terra Moderate Resolution Imaging Spectroradiometer (MODIS) and Cloud and Earth's Radiant Energy System (CERES) data, Zhang et al., (2005b) derived the spatial distribution of SWARE over global oceans. In that study, the perturbations in Top-of-Atmosphere (TOA) SW energy due to aerosol particles are estimated using Terra CERES observations. The Terra CERES observations have a large footprint of ~20 km at nadir (Wielicki et al., 1996). Thus, collocated finer resolution Terra MODIS observations are used for cloud-clearing and ~~reporting finer scale aerosol optical properties detecting aerosol plumes~~ within the CERES field of views (Christopher and Zhang, 2002b; Zhang et al., 2005a;b).

Terra MODIS, CERES, and Multi-Angle Imaging Spectroradiometer (MISR; Kahn et al., 2010) instruments have been continuously observing Earth's atmosphere for more than 16 years (2000-2016). Similarly, the MODIS and CERES instruments on board the Aqua satellite have also been in operation for 14 years (2002-2016). ~~These datasets derived from sensors onboard the Terra and Aqua satellites are long enough to enable climatological analyses of the longer-term variations in both aerosol concentrations and aerosol-induced SW direct climate forcing.~~ Taking advantage of these longer term datasets from the Aqua and Terra satellites, several studies have already examined temporal variations in AOT both on regional and global scales

69 (e.g., Zhang and Reid, 2010, Hsu et al., 2012; Li et al., 2014; Alfaro-Contreras, 2016, Toth et al.,
70 2016). For example, using 10 years (2000-2009) of Collection 5 (C5) Terra and Aqua MODIS
71 Dark Target (DT) AOT data, Zhang and Reid, (2010) found a negligible AOT trend over global
72 oceans, but documented three regions with statistically significant increases in aerosol loadings,
73 including the Indian Bay of Bengal, the Arabian Sea, and the eastern coast of China. Several
74 other studies have also investigated AOT trends using ground-based Aerosol Robotic NETwork
75 (AERONET) data (Li et al., 2014), space borne lidar observations (Toth et al., 2016) and other
76 passive-based observations or model simulations such as Sea-Viewing Wide Field-of-View
77 Sensor (SeaWiFS, Thomas et al., 2010; Mishchenko et al., 2012; Hsu et al., 2012; Zhao et al.,
78 2013; Chin et al., 2014).

79 Still, to our knowledge, SWARE trends have not been studied with the use of both Terra and
80 Aqua data sets. In addition, the new Collection 6 (C6) MODIS aerosol products have changed
81 the magnitudes of global AOT fields significantly (Levy et al., 2013). Thus, in this study, using
82 C6 MODIS and MISR aerosol products, as well as CERES data, we studied AOT and SWARE
83 trends over global oceans with a goal of exploring the following scientific questions:

- 84 1) To what extent have trends changed with the update from MODIS C5 to C6?
- 85 2) What are the regional and global AOT trends over global oceans with the use of near the
86 full Terra/Aqua MODIS and Terra MISR data records?
- 87 3) What are the regional and global trends in MODIS and CERES-based SWARE (Note that
88 although MODIS data are used for cloud clearing, CERES inferred SWAREs are independent of
89 forward calculations of MODIS and MISR)?
- 90 4) What are the instantaneous SW aerosol direct forcing efficiencies and SWARE values on
91 both regional and global scales using near the full Aqua and Terra data records?

5) Can cohesive conclusions (trend patterns) be achieved among passive-, active-based AOT as well as SWARE trend analyses?

This paper is organized as follows. Data used in this study are described in Section 2. In Section 3, differences in AOT trends using C5 and C6 MODIS DT aerosol products are examined for the study period of 2000-2009, and then AOT trends are further derived with the use of near full Terra MODIS and MISR (2000-2015) as well as Aqua MODIS (2002-2015) data records. In Section 4, regional and global SW aerosol direct forcing efficiencies, magnitudes of SWAREs, as well as trends in SWARE are studied using collocated CERES and C6 MODIS DT aerosol products over global oceans. An uncertainty analysis in the derived SWARE trends is also carried in section 4. In Section 5, regional-based AOT and SWARE trends derived from this study are inter-compared with aerosol trend analyses estimated from several other studies that use the CALIOP, MODIS and MISR instruments. Conclusions and discussions are provided in Section 6.

2. Datasets

Eight satellite data sets are included in this study (also shown in Table 1). Regional and global over ocean AOTs were extracted from C6 Terra (MOD04_L2, 2000-2015), Aqua (MYD04_L2, 2002-2015) MODIS DT level-2 aerosol products (Levy et al., 2013) and Version 22 MISR (2000-2015; [Kahn et al., 2010](#)) aerosol products. The Edition 3 Terra and Aqua CERES ERBElke (ES-8; Barkstrom and Wielicki, 1996) and [the Edition 3A](#) CERES Single Satellite Footprint (SSF; Loeb and Kato, 2002) Level 2 swath products provide instantaneous broadband SW fluxes. CALIOP Level 2 5-km cloud layer products (Winker et al., 2010) are also used to assist the cirrus cloud-related analysis.

115 | 2.1 MODIS DT aerosol products: The over ocean C6 MODIS DT aerosol products provides
 116 | ~~spectral AOT at seven wavelengths include spectral AOT retrievals at seven wavelengths~~
 117 | ranging from visible to Shortwave Infrared at a 10 km nadir spatial resolution, with an increased
 118 | ~~pixel size~~resolution of 20x48 km near the edge of the swath (Levy et al., 2013). Only the 550
 119 | nm AOT products are used in this study. Compared to the over ocean C5 MODIS DT products,
 120 | aside from changes in upstream products such as L1B reflectance, geolocation, land/sea and
 121 | cloud mask, one major change included in the over ocean C6 MODIS DT data is the use of non-
 122 | static near surface wind speeds in the retrieval process (Levy et al., 2013). In this study, only
 123 | AOT retrievals with a Quality Assurance (QA) flag of marginal confidence or higher are used.
 124 | The reported uncertainty in AOT data is on the order of $(-0.02 \cdot \text{AOT} - 10\%)$, $(+0.04 \cdot \text{AOT} +$
 125 | $10\%)$ (e.g. Levy et al., 2013), although several studies suggest that higher uncertainties could be
 126 | found for individual retrievals (e.g., Shi et al., 2011).

127 | 2.2 MISR aerosol products: On board the Terra satellite platform, the MISR instrument
 128 | provides observations at nine different viewing zenith angles ($\text{VZA} = 0$ (nadir), $\pm 26.1^\circ$, $\pm 45.6^\circ$,
 129 | $\pm 60.0^\circ$, $\pm 70.5^\circ$) at four different spectral bands ranging from 446 to 866 nm, although like
 130 | MODIS we focus on the green wavelength here (558 nm). Even though MISR has a much
 131 | narrower swath of ~360 km in comparison to MODIS (Diner et al., 2002), the multi-angle
 132 | observations from MISR enable a more reliable AOT retrieval over bright scenes such as desert
 133 | regions (Kahn et al., 2010). Thus, unlike the MODIS and CERES-based analyses in this study,
 134 | which focus on global oceans, trend analyses from MISR include both land and ocean regions,
 135 | unless otherwise stated.

136 | 2.3 CERES SSF products and issues: The CERES SSF data are constructed through weighted
 137 | averaging of MODIS aerosol and cloud retrievals within a CERES footprint based on CERES

138 point spread function (PSF, Loeb et al., 2003; Geier et al., 2003). The CERES instrument
139 measures TOA broadband radiance, to convert from radiance to flux, angular distribution models
140 (ADMs) are needed (e.g. Loeb et al., 2003). For the CERES SSF products, CERES ADMs
141 (Loeb et al., 2003) are used to convert CERES radiance to flux. Over cloud free oceans, AOT is
142 accounted for in CERES ADMs through the use of the radiative transfer modeled anisotropic
143 factors, stratified as sea salt AOT values (Loeb et al., 2003), without considering the impacts of
144 absorbing aerosols. The CERES SSF data cannot be directly used in this study, however, simply
145 because it is constructed with the MODIS products in active production at the time of data
146 collection. That is, both Collection 4 (C4; before April 2006) and C5 (after April 2006) MODIS
147 DT aerosol data were used in constructing CERES SSF data
148 (<http://ceres.larc.nasa.gov/products.php?product=SSF-Level2>). This creates a problem for using
149 CERES SSF in trend analysis, as changes are expected in both global and regional estimations of
150 AOTs between C4 and C5 MODIS DT aerosol products. In addition, C6 MODIS aerosol data,
151 which are currently available, are not included in the CERES SSF data for the study period.
152 Thus, the CERES SSF data are used in this study by collocating with CERES ES-8 and C6
153 MODIS DT data, which are explained in detail later.

154 *2.4 CERES ES-8 products:* The CERES ES-8 data are also available for the near full Terra
155 and Aqua data records. The CERES ES-8 data are constructed by using ADMs from the Earth
156 Radiation Budget Experiment (ERBE)-like algorithm (Suttles et al., 1988). No aerosol
157 properties are considered in constructing ERBE ADMs ~~and aerosols are usually classified either~~
158 ~~as clear or partly cloudy pixels~~. Thus, CERES ES-8 data are used for evaluating the impact of
159 ADMs on CERES derived SWAREs, and for inter-comparison with CERES SSF-based analyses
160 in this study.

2.5 Collocated CERES SSF, ES-8 and MODIS DT products: CERES SSF, CERES ES-8 and

C6 MODIS DT datasets were collocated in this study using 14 years of Aqua and 16 years of Terra data. This is achieved by collocating CERES SSF and ES-8 data as the first step. Note that CERES SSF data include geolocations at surface yet CERES ES-8 data report geolocations at TOA, thus, the collocation is performed by selecting pairs of pixel-level data points from both products that are in the vicinity of each other (less than 2 degree Latitude/Longitude) and have identical raw observations (CERES upward “TOT filtered radiance” and “SW filtered radiance”). Also, CERES SSF reported “Clear area percent coverage at subpixel resolution” values, which are used to define the clear area percentage (CP) in this study, are applied as the initial cloud screen method. Only collocated CERES SSF / ES-8 pairs that have CP values of 95% or higher are included in further analyses. -Note that only CERES pixels that have a MODIS reported cloud fraction of 1% or less are used in the final process. A more relaxed CP threshold of 95% is adopted here, partially for studying the impact of cloud contamination on CERES derived SWAREs as shown in Table 5.

As the second step, the collocated CERES SSF and ES-8 data are further collocated with C6 MODIS DT data. Only MODIS and CERES data that are from the same satellite platform are used in the collocation. To collocate MODIS and CERES data, surface geolocations (Latitudes/Longitudes) of both datasets are first identified and the two datasets are collocated in space and time based on the PSF of the CERES instrument (Wielicki et al. 1996, Christopher and Zhang, 2002a;b, Zhang and Christopher, 2003). ~~Also, since MODIS DT products have a spatial resolution of 10 km at nadir, only a~~ arithmetic averages are performed for MODIS data points that are within a CERES footprint.

CERES data are available from three scan modes: the cross-track, rotating azimuth plane scan, and fixed azimuth plane scan modes. To maintain data consistency, only cross track mode CERES data from Terra and Aqua are used in this study. Also, to further screen potential noisy data, only CERES observations with valid SW flux retrievals (from CERES-ES-8 or CERES SSF) and viewing zenith angle (VZA) as well as solar zenith angle (SZA) less than 60 degrees are considered in this study. Over_{land} observations are further excluded in the study by only using collocated pairs that have CERES ES-8 scene ID of “Clear Ocean”, “Partly Cloudy Over Ocean” and “Mostly Cloudy Over Ocean”. Cloud and aerosol properties within a CERES observation are reported based on the collocated C6 MODIS DT products. The following ancillary data are also recorded for each CERES observation: total number of collocated C6 MODIS DT retrievals, number of valid C6 MODIS DT retrievals (with valid cloud fraction and AOT values), number of valid C6 MODIS DT retrievals with QA flags of “marginal”, “good” and “very good”. Lastly, only CERES pixels with CP larger than 99% and a reported MODIS cloud fraction (CF) of less than 1% and are used in this study and the impacts of cloud contamination on the derived SWARE trends are also evaluated later in this paper.

2.6 Collocate CERES ES-8, MODIS DT and CALIOP products: Using collocated CALIOP and MODIS observations, Several studies have suggested that MODIS AOT retrievals may be contaminated with optically thin cirrus clouds (OTC, e.g. Kaufman et al., 2005, Huang et al., 2011, Feng et al., 2011, Toth et al., 2013). ~~Toth et al. (2013) suggests that even MODIS detected cloud free scenes may be contaminated with optically thin cirrus clouds (OTC).~~ To further study the effects of OTC on the trend analysis, the 5 km CALIOP cloud layer product (Winker et al., 2010) is utilized. The CALIOP cloud layer (CAL_LID_L2_05kmCLay) data are spatiotemporally collocated with the already collocated MODIS-CERES data sets on-board the

206 Aqua platform. CALIPSO's Feature Classification Flag is used to locate residual OTC within
207 CERES observations. It should be noted that CALIOP's data record spans only about half of our
208 study period (June 2006 – Dec. 2015) and is available only on the Aqua platform, thus it will be
209 used as a secondary analysis presented in Section 4.2. Note the CERES CALIPSO CloudSat
210 MODIS (C3M) products, which are constructed by collocating CERES SSF, CALIPSO,
211 CloudSat and MODIS data (Kato et al., 2011), are also available from 2006-2011
212 (<https://ceres.larc.nasa.gov/products.php?product=CCCM>). However, the C3M data are not
213 available after 2011. Also, to avoid decoupling the impacts of ADMs and cirrus cloud effects, a
214 simple approach, as mentioned in this section is used in this study.

215 ~~2.7 Estimating trend significance: Lastly, trend significances are computed based on two~~
216 ~~statistical methods. To be consistent with Zhang and Reid (2010), the Weatherhead method~~
217 ~~(Weatherhead et al., 1998, hereafter WH) is used to calculate trend significances for monthly-~~
218 ~~based AOT data. To increase data samples, SWARE values are estimated/averaged on a~~
219 ~~seasonal basis. However, the WH method is applicable to monthly data and thus, the Mann-~~
220 ~~Kendall method (e.g. Mann, 1945; Kendall, 1975) is used to estimate trend significances for~~
221 ~~seasonal-based analyses. For comparison purposes, both methods are applied to the AOT trend~~
222 ~~analysis as mentioned in Sections 3 and 4, wherever applicable.~~

223

224 3. AOT trends from over ocean DT MODIS data

225 To initiate this study, we begin with an update to global trend analyses in AOT. Included are
226 two components. First, we evaluate if recent changes in the MODIS aerosol product affect past
227 conclusions on regional aerosol trends over the globe. This is followed by an extension of the
228 trend analysis to the entire 2000-2015 study period (Section 3.2).

3.1 Update of AOT trends from Collection 5 to Collection 6

In the Zhang and Reid (2010) ~~trend~~-paper, 10 years of C5 DT MODIS over ocean data were used in deriving regional and global AOT trends. With the recent release of C6 Aqua and Terra DT MODIS data, including significant updates to calibration and cloud clearing algorithms, it is worth a short reproduction of this work with current products.

Similar to Zhang and Reid (2010), Level 2 C6 DT over water Terra MODIS data were binned into $1^\circ \times 1^\circ$ (Latitude/Longitude) monthly averages. “Bad” retrievals, as indicated by the QA flag included in the dataset, are discarded from the analysis, as were MODIS cloud fraction above 80% to minimize the effect of cloud contamination (Zhang and Reid, 2010). Using the monthly gridded over-ocean C6 Terra MODIS DT data from 2000-2009 (excluding August 2000 and June 2001 as these months contained less than 20 days of valid data), regional AOT trends, as well as trend significances (based on WH, as suggested from Zhang and Reid, 2010) were derived and are shown in Figure 1a. [Trend significances are computed based on two statistical methods. To be consistent with Zhang and Reid \(2010\), the Weatherhead method \(Weatherhead et al., 1998, hereafter WH\), which account for data autocorrelation, is used to calculate trend significances for monthly-based AOT data. For a comparison purpose, the Mann-Kendall method \(e.g. Mann, 1945; Kendall, 1975, hereafter MK\) is also used. Note that the MK method is also used as it can be applied to estimate trend significances for seasonal-based analysis as discussed in section 4. Both methods are applied in Sections 3 and 4, wherever applicable.](#)

To create Figure 1, data are deseasonalized by removing 10-year averages from any given month, for each grid point. Also, AOT trends are derived only for bins which have more than 72

251 months (60%) of valid data records. In Figure 1a, regions with statistically significant trends at a
252 95% confidence interval (from WH), are highlighted with black dots.

253 To inter-compare AOT trend analysis from Zhang and Reid (2010), AOT trends from 10
254 selected regions, ~~including north west coast of Africa (8°N–24°N, 60°W–18°W), India Bay of~~
255 ~~Bengal (10°N–25°N, 78°E–103°E), eastern coast of China (20°N–40°N, 110°E–125°E),~~
256 ~~Central America (5°N–20°N, 120°W–90°W), Arabian Sea (5°N–23°N, 50°E–78°E),~~
257 ~~Mediterranean Sea (30°N–45°N, 0°–40°E), south west coast of Africa (23°S–7°S, 20°W–~~
258 ~~45°E), eastern coast of North America (30°N–45°N, 80°W–60°W), south east coast of Africa~~
259 ~~(27°–15°S, 32°E–45°E), and southeast Asia (15°S–10°N, 80°E–120°E)~~ are computed as
260 shown in Table 2. Also, suggested from Zhang and Reid (2010), the AOT trend from Remote
261 Ocean (RO, 40° S - 0°, 179° W – 140° W) is used as a proxy for unrealized bias in the AOT
262 trend due to issues such as calibration and signal drifts, as this is the region that is least affected
263 by any major aerosol plumes originated from main continents. ~~For illustrative purposes, the~~
264 ratios and differences in AOT trends for both C6 and C5 Terra MODIS based analysis are also
265 shown in Figs. 1e and 1f, respectively, for the study period of 2000-2009. Only grids with AOT
266 trends above or below ± 0.002 AOT/year are used in this comparison.

267 As suggested from Table 2, both AOT trends and trend significances (based on WH) are
268 similar with the use of C5 and C6 Terra MODIS DT over ocean data for the study period of
269 2000-2009. This suggests that although documentable changes are made to the C6 MODIS DT
270 over ocean data (Levy et al., 2013), the impact of those changes on global and regional AOT
271 trend analysis is rather marginal. For a comparison purpose, Table 2 also includes trend
272 significances derived using the Mann-Kendall method ($|z|$) for the C6 MODIS DT-based
273 analysis, and consistent results are found from both methods a majority of the time.

274 | Lastly, ~~for illustrative purposes,~~ regional and global averages over ocean C5 and C6 Terra
275 | MODIS DT AOTs are also shown in Table 2 for the period of 2000-2009. Note that in Zhang
276 | and Reid (2010), data-assimilation quality C5 MODIS DT data, which is implemented with
277 | extensive QA steps (e.g. Zhang and Reid, 2006; Shi et al., 2011), were used. Here regional and
278 | global mean C5 AOTs are derived using similar steps as were used in constructing the C6 AOT
279 | data, which are differ from the data-assimilation quality C5 MODIS DT data as used in Zhang
280 | and Reid (2010). Still, as suggested from Zhang and Reid (2010), although QA steps could
281 | lower the mean global over ocean AOTs from ~0.15 to ~0.11, in part due to the removal of cloud
282 | contaminated retrievals, minor impacts on the AOT trend analysis are reported. As suggested
283 | from Table 2, a 10% reduction in global mean over ocean AOT is found for the C6 MODIS DT
284 | data in comparing with the C5 data, possibly due to a reduction in marine background AOTs
285 | (e.g., the Enhanced Southern Ocean Anomaly feature, as shown in Toth et al., 2013, no longer
286 | exists in the C6 product).

287

288 | **3.2 AOT trends from near full Terra and Aqua data records**

289 | Extending the analysis from the previous section, AOT trends are evaluated for the near full
290 | available data record (March 2000 – December 2015 for MODIS Terra and MISR, and July 2002
291 | – December 2015 for MODIS Aqua) of C6 over ocean MODIS DT and MISR aerosol products.
292 | The C6 MODIS DT data are processed and filtered with the same steps as mentioned in section
293 | 3.1 to construct $1^\circ \times 1^\circ$ (Latitude/Longitude) monthly averages for trend estimates. MISR
294 | products are also binned into monthly-averaged $1^\circ \times 1^\circ$ degree bins and filtered according to
295 | Zhang et al., (2017 submitted).

Figure 2 depicts the C6 MODIS Terra (Fig. 2a), C6 MODIS Aqua (Fig. 2b) and v22 MISR (Fig. 2c)-based global aerosol distributions (Latitude: -60° to 60°) using monthly gridded AOTs. Only those bins with more than one thousand data counts were considered for this analysis ([this is an arbitrary threshold selected for removing some over land water retrievals over scenes such as lakes. It is also partially used for ensuring sufficient data are included in the trend analysis](#)). ~~A quick-comparison between~~ Figs. 2a and 2b shows a high level of similarity over most of the globe, which is consistent with what has been reported by Remer et al. (2006) using 3 years of C5 MODIS data. Similar spatial patterns are also found for MODIS- and MISR-based AOT analyses over global oceans (Figure 2c). This is further confirmed from Figures 2d and 2e, which show the ratios and the differences between Terra MODIS and Terra MISR AOTs. Still, the band of high AOT over the southern oceans, which is identified as a potential artifact in both C5 MODIS and MISR aerosol products that may be due to cloud contamination (Toth et al., 2013), is no longer apparent in the C6 MODIS DT aerosol products.

Using data shown in Figure 2, the time series of over ocean global mean AOT are also examined and shown in Fig. 3. Figure 3a shows the monthly-averaged C6 MODIS Aqua (red), MODIS Terra (blue) and MISR (green) AOTs over global oceans for the entire time frame of each data set. It should be noted that over land observations from MISR are not included in global averages in order to get a more direct comparison with the over ocean MODIS DT aerosol data sets. Monthly-variations in globally-averaged ([simple arithmetic mean](#)) AOTs can be observed, with the solid lines showing the AOT trends for the entire time period for each sensor. Similar to Zhang and Reid (2010), the lowest monthly-averaged MODIS AOTs are found during the Northern-Hemispheric winter months while the highest aerosol loading activity over global oceans seems to occur during the Northern-Hemispheric spring and summer months.

Formatted: Not Highlight

319 Figure 3b shows AOT anomalies after deseasonalizing the monthly data shown in Figure 3a.
320 ~~Interestingly,~~ Terra MODIS and MISR show trends of differing signs; a statistically significant
321 increase/decrease in monthly-mean AOT values of 0.008/-0.005 AOT decade⁻¹ is found when
322 using Terra MODIS/MISR data for the study period of 2000-2015. In comparison, a statistically
323 insignificant global over ocean AOT trend is found to be 0.0003 AOT decade⁻¹ using Aqua
324 MODIS data for the study period of 2002-2015. A trend difference is clearly seen even if we
325 restrict all datasets to the same study period of 2002-2015, which could be an indication of
326 potential calibration related issues with one or all of the sensors.

327 Zhang and Reid et al., (2010) suggested that since the remote oceans region (defined in Table
328 2) is least affected by major continental originated aerosol plumes, the AOT trend from this
329 region may be used for checking calibration related issues or some other unrealized uncertainties
330 originated from the upstream data used. A caveat here is that we assumes that the calibration
331 degradation propagates linearly into AOT. The correction might therefore be an under/over-
332 correction in those higher-AOT areas. Similar to Fig. 3b, Fig. 3c depicts the monthly-averaged
333 deseasonalized AOTs over the remote ocean region where the monthly anomalies and trend lines
334 are visible. Similar to Zhang et al. (2017), an insignificant trend of 0.0003 AOT decade⁻¹ is
335 found for the remote ocean region using Aqua MODIS data, while a statistically significant
336 (Weatherhead method) trend of 0.006/-0.004 AOT decade⁻¹ is found for the same region with the
337 use of deseasonalized Terra MODIS/MISR data. Those differences in AOT trends are not
338 surprising. For example, a recent study suggests a potential cross-talk among Terra MODIS
339 thermal channels, which will affect MODIS cloud detection (Moeller and Frey, 2016) and
340 correspondingly, Terra MODIS AOT trends. Similarly, Limbacher and Kahn, (2016) reported an
341 up to 2% decrease in MISR signals from 2002-2014 that could affect MISR AOT trends. AOT

trends estimated from this study are henceforth adjusted based on AOT trends detected from the Remote Ocean region; this is done to reduce potential impacts from upstream data used in the AOT retrievals by assuming that a near zero AOT trend should be observed over the remote ocean region (shown in Table 3).

Using monthly gridded data, AOT grid-level trends are also estimated on a global scale, for MODIS Terra- (Fig. 1b), MODIS Aqua- (Fig. 1c) and MISR (Fig. 1d)-based analysis for the entire data record period. Again, the black-dotted areas on the map are for regions with statistically significant trends at a 95% confident interval estimated using the WH method. When comparing with the 10-year analysis as mentioned in Section 3.1 (Fig. 1a), some similarities are clearly visible. For example, increasing AOT trends are observed over the Arabian Sea and Indian Bay of Bengal, while decreasing trends are observed over the Mediterranean Sea and east coast of US from both Figures 1a and 1b. Still for some regions, such as over coastal China, Fig. 1a shows a positive AOT trend, yet near zero AOT trend is found in Figure 1b. A recent study suggests a possible increase in AOT from 2000-2007 over coastal China, followed by a decreasing trend from 2008-2015 (Zhang et al., 2017), which can be used to explain the differences as observed in Figure 1 over coastal China. Likewise, regional analyses are also conducted as documented by Table 3 and Figure 4. In addition to the regions reported by Zhang and Reid (2010), two regions have been added to the study which include Persian Gulf (24° N – 30° N, 50° E – 60° E) and Red Sea (15° N – 30° N, 30° E – 45° E). All regions are outlined by black boxes in Fig. 1.

Unlike the insignificant AOT trends on the global scale, both statistically significant positive and negative trends are found for several regions as shown in Figure 4 (as well as Table 3). For example, statistically significant positive AOT trends (where statistically significant trends are

denoted by bold font on Table 3) are found from all three datasets (Terra and Aqua MODIS DT and MISR over water aerosol products) over the Bay of Bengal (Fig. 4a), Arabian Sea (Fig. 4b) and Red Sea (Fig. 4d). Note that both the Bay of Bengal and Arabian Sea have been identified in Zhang and Reid (2010) as regions with statistically significant positive trends for the study period of 2000-2009. However, the rates of increase of aerosol loading have [plausibly](#) slowed down over the last five years for both regions, indicated by ~20-30% reductions in AOT trends when estimated using the near full Terra data records. [Flattening of AOT trends with respect to time can also be observed in Fig. 4 for both regions for 2010-2015.](#) The Red Sea and Persian Gulf are newly introduced for this study but seem to show the highest increase in aerosol loading during the study period (as derived from Terra data). This increase in AOT has been attributed to a number of mechanisms, including a trend in surface wind, precipitation, and soil moisture (Al Senafi and Anis 2015; Klingsmuller et al, 2016), as well as a climatological deepening of the summertime monsoonal low over the Arabian Sea (Solmon et al., 2015). Statistically significant negative trends are found over the Mediterranean Sea (Fig. 4f) and the east coast of N. America (Fig. 4g), again from all three datasets. These findings are also consistent with what has been reported by Toth et al. (2016) with the use of CALIOP data. Also, despite the differences in sampling methods as well as calibration, regional trends from MISR are similar to trends derived using both Aqua and Terra MODIS DT data.

4. SWARE Trends

In Section 3, changes in aerosol concentrations over global oceans are studied with respect to AOT trends. The temporal variations in aerosol concentrations could also introduce changes in TOA SW fluxes and thus can be detected using collocated MODIS and CERES (SSF and ES-8)

observations. In this section, the SWARE trends derived using MODIS and CERES (SSF and ES-8) data are explored and are inter-compared with AOT trends as mentioned in the previous section.

391

392 **4.1 SWARE trend Analysis using collocated MODIS and CERES data**

393 In several past studies, SWARE values are derived using collocated CERES and MODIS
394 data based on equation 1 (e.g. Loeb and Kato, 2002; Loeb et al., 2003; Zhang et al., 2005b;
395 Christopher and Zhang., 2002a;b):

$$396 \quad SWARE = F_{clear} - F_{aero} \quad (1)$$

397 where F_{clear} represents the TOA SW flux over aerosol and cloud free skies and F_{aero} represents
398 the TOA SW flux over cloud free skies. Taking the derivative of equation 1 with respect to time,
399 we can obtain equation 2:

$$400 \quad \frac{\partial SWARE}{\partial t} = \frac{\partial F_{clear}}{\partial t} - \frac{\partial F_{aero}}{\partial t} \quad (2)$$

401 Here $\partial SWARE / \partial t$ represents the trend in SWARE. $\partial F_{aero} / \partial t$ represents a temporal change in
402 TOA observed SW flux over cloud free skies. $\partial F_{clear} / \partial t$ represents a change in background TOA
403 SW energy over cloud and aerosol free skies. Here F_{clear} is a function of viewing geometry (e.g.,
404 solar zenith angle) and near surface wind patterns. By deseasonalizing CERES SW flux data, we
405 can remove the solar zenith angle effect. Also, by using monthly averages of instantaneous
406 retrievals, we assume that there is no viewing zenith or azimuth dependency with respect to time.
407 If we further assume that the changes in near surface wind patterns are negligible for the study
408 period, the $\partial F_{clear} / \partial t$ term can be assumed to be near zero (the impact of near surface wind speed
409 on the SWARE trend is explored in a later section). Thus, we can rewrite equation 2 as:

$$410 \quad \frac{\partial SWARE}{\partial t} = \frac{-\partial F_{aero}}{\partial t} \quad (3)$$

411 As suggested from equation 3, the trends in SWARE can be directly estimated from the temporal
412 variations in SSF/ES-8 TOA SW flux from CERES over cloud free skies (less than 1% cloud
413 fraction and larger than 99% CP). This approach avoids the need for estimating F_{clear} , which
414 cannot be observed and can only be derived through radiative transfer calculations (Christopher,
415 2011) or extrapolation (e.g., there is always a positive definite AOT).

416 The cloud-free TOA SW fluxes are obtained from CERES (SSF and ES-8) data in this study.
417 This is accomplished by utilizing the collocated MODIS-CERES (SSF and ES-8) data set. As
418 mentioned in Section 2, only those MODIS observations over cloud-free scenes ($CF < 1\%$ and
419 $CP > 99\%$) are used for this analysis as SW flux is sensitive to cloud contamination (Zhang et
420 al., 2005a;b). However, filtering the MODIS data sets with such strict cloud fraction criteria
421 significantly reduces the data volume, which may lead to a sampling bias when working with the
422 MODIS-CERES data set (e.g., Zhang and Reid 2009). Therefore all MODIS-CERES data sets
423 have been averaged into seasons as opposed to monthly averages. In addition, the MODIS-
424 CERES collocated observations are gridded into $2^\circ \times 2^\circ$ (Latitude/Longitude) grids to further
425 alleviate the sampling bias produced by the data reduction in the MODIS-CERES data set.

426 Figure 5 shows the spatial distributions of AOT and cloud-free CERES TOA SW flux over
427 global oceans using collocated MODIS-CERES data (2000-2015 for Terra and 2002-2015 for
428 Aqua). Comparing Figs. 5a and 5b with Figs. 2a and 2b, Terra (5a) and Aqua (5b) AOT plots
429 generated using the collocated MODIS-CERES data are similar to the spatial distributions of
430 AOT generated using the original Terra and Aqua C6 MODIS DT data. Figures 5e and 5f show
431 the gridded cloud-free CERES SSF TOA SW fluxes for Terra and Aqua, respectively. It is
432 interesting to note that the spatial distributions of MODIS AOT and cloud free CERES SSF TOA
433 SW flux (SW_{ssf}), although from two different instruments that measure different physical

quantities (narrow band versus broadband energy; dependent versus independent of forward calculations of MODIS), show remarkably similar patterns.

Similar to Figs. 5e and 5f, Figs. 5c and 5d show the gridded cloud-free TOA SW fluxes for Terra and Aqua respectively, but with the use of CERES ES-8 SW fluxes. Again, the spatial patterns of cloud-free CERES ES-8 TOA SW flux (SW_{es8}) highly correlate with AOT spatial patterns. Still, an overall difference in CERES SSF and ES-8 TOA SW fluxes is clearly observable (Figs. 5g and 5h) and SW_{ssf} values are generally $8-9 \text{ Wm}^{-2}$ higher than SW_{es8} values. Smaller than average differences in cloud free TOA SW fluxes between the two products can be seen over dust aerosol polluted regions such as the northwest coast of Africa, while larger than average differences are found over regions such as east coast of Asia, west coast of South America and Southeast Asia where other type of aerosol particles dominate. For illustrative purposes, data counts for each $2 \times 2^\circ$ (Latitude/Longitude) bin that are used to create Figs. 5a-h are also shown in Figs. 5i and 5j for Aqua and Terra respectively.

The relationship between AOT and cloud free TOA SW flux values from Fig. 5 is also evaluated in Figs. 6 and 7 and Table 4. As suggested from Fig. 6a (Aqua) and 6c (Terra), multi-year means of AOTs and SW_{ssf} values share a highly correlated (correlations of 0.72 and 0.73 for Aqua and Terra data, respectively), non-linear relationship. Similar but higher correlations between multi-year mean AOT and SW flux values are also found when using CERES ES-8 data (correlations of 0.83 and 0.87 for Aqua and Terra data, respectively) as shown in Figs. 7a (Aqua) and 7c (Terra).

Figure 6b shows the Aqua MODIS AOT and Aqua SW_{ssf} relationship ([non-linear](#)) for 5 selected regions that have high regional AOT values (e.g., maximum bin averaged AOT > 0.3), including the southwest and northwest coasts of Africa, coastal China, India Bay of Bengal, and

457 Arabian Sea. In particular, a much lower slope of 37.8 Wm^{-2} per AOT is found for the
 458 southwest coast of Africa region in-comparing with the other four regions. A similar pattern is
 459 observed for using Terra CERES SSF data (slope of 42.5 Wm^{-2} per AOT for the southwest coast
 460 of Africa region) as well as for using both Aqua and Terra CERES ES-8 data (slopes of 39.8 and
 461 43.7 Wm^{-2} per AOT for Aqua and Terra respectively, for the southwest coast of Africa region).
 462 Note that the slope of AOT and SW flux is a measure of (inversely proportional to) the
 463 instantaneous SW aerosol direct forcing efficiency. Smoke aerosol particles dominate high
 464 AOTs for the southwest coast of Africa region, while other regions are also influenced by non-
 465 smoke aerosols such as dust aerosol particles. Thus Figs. 6 and 7 suggest a lower SW forcing
 466 efficiency (in magnitude) for biomass burning aerosols, in part due to a stronger absorption at the
 467 visible spectrum (e.g., Remer et al., 2005).

468 We have further explored the topic by estimating SW aerosol forcing efficiencies for the
 469 Dec.-May and Jun.-Nov. seasons as shown in Table 4. As indicated in Table 4, SW aerosol
 470 direct forcing efficiencies may experience a seasonal dependency such as over the Coastal China
 471 region. For example, a CERES SSF-based aerosol SW forcing efficiency value of -88.3 Wm^{-2}
 472 per Aqua MODIS AOT is found for the coastal China region for the Dec.-May period. A lower
 473 value (CERES SSF-based) of -74.7 Wm^{-2} per Aqua MODIS AOT is found for the Jun.-Nov.
 474 season for the same region. Similar conclusions can also be found using Terra data as well as
 475 using CERES ES-8 data. The seasonal dependency in SW aerosol forcing efficiency is not
 476 surprising for the coastal China region, as dust aerosols are expected for the spring season, while
 477 pollutant and smoke aerosols likely dominate for the Jun.-Nov. study period (Zhang et al., 2017).
 478 In comparison, less seasonal-based changes are found for the Arabian Sea region, which may be
 479 plausibly linked to less significant temporal variation in aerosol speciation over the region. Also

480 indicated in Table 4, the derived SWARE has a strong regional-dependency, while the multi-year
481 averaged SWARE is around -6 to -7 Wm^{-2} for the southwest coast of Africa region, over the
482 coastal China region, SWARE values of below -20 Wm^{-2} are found. Note that this conclusion
483 remains unchanged regardless of using Terra or Aqua data, or using CERES ES-8 or SSF ADMs.

484 Over global oceans, the multi-year mean instantaneous SW aerosol direct forcing efficiencies
485 are estimated to be -61 (-58) and -58 (-58) Wm^{-2} per AOT using Aqua and Terra CERES SSF
486 (ES-8) data, respectively. Those numbers are lower than -70 Wm^{-2} per AOT, which is reported
487 from a previous study (Christopher and Jones, 2008). We suspect that the differences in forcing
488 efficiency values may be introduced by different data screening methods as well as a much
489 longer study period. Still, using estimated forcing efficiencies as well as AOTs (Table 4), the
490 global mean (14 years of Aqua and 16 years of Terra data) over oceans SWARE values are
491 found to be around -7 Wm^{-2} regardless of datasets (Terra or Aqua) and ADMs (SSF or ES-8)
492 used. Note that regional and global mean AOTs as shown in Table 4 are derived using the
493 collocated MODIS and CERES datasets, representing mean AOTs over CERES cloud-free skies.
494 Thus, mean AOTs as reported from Table 4 are different from AOTs as included in Table 2.

495 With the use of seasonally gridded SW flux values, the times series of cloud-free sky CERES
496 SSF and ES-8 TOA SW flux over global oceans are investigated and depicted in Fig. 8a, and the
497 corresponding deseasonalized cloud-free sky flux anomalies are show in Fig. 8b. While Fig. 8a
498 suggests an $\sim 8 \text{ Wm}^{-2}$ difference in mean over ocean cloud-free sky SW flux between CERES
499 SSF and ES-8 products, a small difference in cloud-free sky SW flux trend of 0.2 - 0.3 Wm^{-2}
500 decade^{-1} is found (Fig. 8b) between the two products for both Terra and Aqua data. For example,
501 negative trends on the order of -0.50 Wm^{-2} and -0.26 Wm^{-2} per decade are found for using Aqua
502 CERES ES-8 and SSF products respectively. Also, although larger cloud-free sky SW flux

503 trends in magnitude are found when using Terra data, the difference between CERES SSF-based
504 and CERES ES-8-based trends is still on the order of $0.2 - 0.3 \text{ Wm}^{-2} \text{ decade}^{-1}$ (Cloud-free sky
505 SW flux trend is $-1.50 \text{ Wm}^{-2} \text{ decade}^{-1}$ for Terra CERES ES-8 data and is $-1.22 \text{ Wm}^{-2} \text{ decade}^{-1}$ for
506 Terra CERES SSF data). Figures 8a and 8b may imply that different ADMs could significantly
507 impact the derived SW flux values, but their impact on cloud-free sky TOA SW flux trends are
508 rather marginal.

509 Similar to Section 3, we used CERES SW flux trends over the remote ocean region as
510 indicators for potential radiometric calibration related issues. The deseasonalized CERES SSF
511 (ES-8) SW trends over the remote ocean regions (Fig. 8c) seem to suggest plausible artificial
512 trends of $-0.25 (-0.50) \text{ Wm}^{-2} \text{ decade}^{-1}$ for Aqua and $-0.70 (-0.92) \text{ Wm}^{-2} \text{ decade}^{-1}$ for Terra,
513 although these trends are also affected by various uncertainties that are further explored in a later
514 section. To examine if we could observe similar issues with the use of full CERES SSF / ES-8
515 datasets, Fig. 9 shows the all sky CERES flux trend for the same study periods as Fig. 8.
516 Decadal changes of SSF (ES-8) all sky flux are less than $0.5(0.7) \text{ Wm}^{-2}$ and $0.4(0.5) \text{ Wm}^{-2}$ for
517 Terra and Aqua data, respectively. The Aqua all-sky flux trends are comparable to cloud-free
518 sky trends for both SSF and ES-8 fluxes. However Terra-based all sky trends are much lower in
519 magnitude than the corresponding cloud-free flux, which indicates that cloud-free sky CERES
520 SW energy may be more sensitive to calibration related issues than all sky flux data for Terra–
521 based analysis only. Still, if we account for the changes in SW trends over the remote ocean
522 region, a negligible SW flux (SWARE) trend for Aqua and a negative (positive) SW flux
523 (SWARE) trend of $-0.5 \text{ Wm}^{-2} \text{ decade}^{-1}$ ($0.5 \text{ Wm}^{-2} \text{ decade}^{-1}$) for Terra can be estimated for the
524 global oceans from collocated MODIS-CERES data.

~~Surprisingly, Although~~ different cloud-free sky SW flux trends are found while using CERES ES-8 data, after adjusting the detected trends with trends from remote oceans, a zero SW flux (SWARE) trend is found while using collocated Aqua ES-8 SW fluxes from the MODIS-CERES data and a negative (positive) SW flux (SWARE) trend of $-0.6 \text{ Wm}^{-2} \text{ decade}^{-1}$ ($0.6 \text{ Wm}^{-2} \text{ decade}^{-1}$) is found using collocated Terra ES-8 SW fluxes from the MODIS-CERES collocated data, both are in good agreement with values estimated using the SSF SW fluxes from the same data. This again may seem to suggest that the impact of ADMs on SWARE trends over global oceans estimated from the collocated MODIS and CERES data are rather marginal.

A regional trend analysis for the deseasonalized cloud-free sky SSF and ES-8 SW fluxes is also carried out and presented in Table 3 and Figure 10. A good agreement is shown between regional trends of AOTs (Fig. 4) and cloud-free fluxes (Fig. 10) for a majority of the regions (also shown in Table 3 for a direct comparison). For example, statistically significant positive (based on the Mann-Kendall method) SW flux trends are found over the Arabian Sea, and statistically significant negative trends are found over the Mediterranean Sea and eastern US coast for both Aqua and Terra-based analyses. Also, over the east coast of China, although a near positive trend is found for the study period of 2000-200~~68~~ (Terra), the SW flux trend turns negative from 200~~69~~-2015 (Figure 11). This is consistent with what has been reported for AOT trends from a recent study (Zhang et al., 2017) as well as in Section 3. Here a piecewise linear fit method from Tomé and Miranda (2004) is applied to detect turning points in trends, similar to what is suggested by Zhang et al. (2017). Also, similar to Zhang et al. (2017), we assume a minimum of 36 months between any two detected turning points. For regions such as the Bay of Bengal, although positive SW flux trends are found, the trends are not statistically significant for one or all datasets.

Next, the grid-level AOT and cloud-free flux trends are derived from the collocated MODIS-CERES data sets as shown in Fig. 12. Figures 12a (Terra) and 12b (Aqua) depict the de-biased (applied corrections based on the estimate from the remote ocean region) changes in deseasonalized AOT per year for each $4^\circ \times 4^\circ$ (Latitude/Longitude) grid (averaged from the $2^\circ \times 2^\circ$ Latitude/Longitude dataset) over the entire time period (all seasons and years combined). Figures 12e and 12f depict the grid level CERES SSF SW flux trends over cloud-free skies similar to Figs. 12a and 12b. Similar to the AOT grid level analysis shown in Fig. 1, at least 60 percent of the data record in each grid are required to have valid AOT and SW flux trend values. Comparing between Aqua AOT (Fig. 12b) and CERES SSF cloud free SW (Fig. 12f) trends, similarity can be found. For example, positive trends are found, from both plots, over coastal Indian and the Arabian Sea regions, and negative trends are observable from Europe and the east coast of North America. The similar conclusion can also be reached when using Terra data (Figs. 12a and 12e) as well as when using CERES ES-8 data (Figs. 12c and 12d). Still discrepancies can be found. For example, although the spatial distributions of AOT from both Terra and Aqua show similar patterns, differences between the spatial distributions of Terra and Aqua CERES cloud-free SW fluxes, regardless of ADMs used, are clearly visible. Much larger regions with negative cloud free SW flux trends are found for using Terra data. This may be a result of several possible issues such as SW flux outliers in the CERES data set, quality control applied to the CERES data set, or cloud contamination issues. Thus, this will be examined in the following section.

4.2 Uncertainty in Cloud-Free Flux Trend Analysis

570 In this section, issues that could impact the derived SWARE trends are explored, which
571 include changes in near surface wind patterns, cloud contamination, and uncertainties in the
572 cloud free SW flux trend estimates over the remote ocean region (used as a proxy for radiometric
573 calibration). Note that there are other uncertainty sources that may impact the derived CERES
574 SW flux values, such as uncertainties in converting unfiltered to filtered radiances (Zhang et al.,
575 2005b). However, temporal variations of those uncertainty sources are assumed to be negligible
576 for this study, and thus those terms are not included in the trend uncertainty analysis.

577 *4.2.1 Baseline region (a proxy for radiometric calibration):* As mentioned in Section 4.1, the
578 TOA cloud-free SW flux trend over the Remote Ocean region is used as an indicator for
579 potential calibration related issues. The selection of the Remote Ocean region boundaries is
580 rather arbitrary, and thus the variations in TOA cloud-free CERES SW flux trends over the
581 remote ocean region are investigated by modifying the regional boundaries for four different
582 scenarios as shown in Table 5. Alternate remote ocean regions are chosen by shifting the
583 original boundaries by 10 degrees in each direction. The variations in estimated CERES SSF
584 (ES-8) SW flux trends, which correspond to standard deviation values of 0.08 (0.09) and 0.03
585 (0.08) $\text{Wm}^{-2} \text{decade}^{-1}$ for Terra and Aqua, respectively, provide the first order estimation of the
586 potential variations in the estimated SW trends over the remote oceans.

587 *4.2.2 Cloud fraction:* Similarly, the cloud-free SW flux trends over global oceans are estimated
588 through varying MODIS cloud fractions from 0 to 5% as indicated in Table 5. The standard
589 deviation of the data spread is found to be less than 0.1 $\text{Wm}^{-2} \text{decade}^{-1}$ for both Terra- and Aqua-
590 based CERES SSF and ES-8 SW flux trend analyses, suggesting that cloud contamination has a
591 minor effect on the trend analysis. This conclusion is also confirmed by a sensitivity test by
592 estimating SSF and ES-8 SW flux trends through varying CP values from 95% to 100%.

593 *4.2.3 Thin Cirrus:* Through the use of CALIOP observations, several studies suggest that OTC
594 cloud contamination exists in MODIS detected totally cloud free skies (e.g., Toth et al., 2013).
595 Therefore, the impacts of OTC clouds are evaluated by collocating CALIOP cloud layer data
596 with the already collocated Aqua MODIS and CERES data pairs. All CALIOP observations are
597 spatiotemporally collocated with the current original CERES observation if the temporal
598 difference in the two sensor's scan times is less than or equal to five minutes and if the center of
599 the CALIOP observations lies within 0.3 degrees of the center of the CERES observations. All
600 collocated CERES observations are assigned a cirrus cloud flag depending on whether any of the
601 collocated CALIOP pixels was found to be contaminated by cirrus clouds. The global averaging
602 process is once again performed using the collocated MODIS-CERES-CALIOP observations.
603 CERES observations which are contaminated by cirrus clouds, as identified by CALIOP data,
604 are removed from the averaging process. The resulting global AOT and cloud-free flux trends
605 are presented in Figs. 13a and 13b, respectively for using both CERES ES-8 and SSF SW fluxes.
606 For comparison, the MODIS-CERES trends are also shown (red) over the same time period
607 (summer 2006 – fall 2015). Despite differences in globally averaged AOTs, the global TOA SW
608 flux trends derived using the two different data sets are remarkably similar. The standard
609 deviation in global cloud-free CERES SSF flux trend calculations due to OTC is less than 0.1
610 $\text{Wm}^{-2} \text{ decade}^{-1}$, as shown in Table 5. Thus, OTC clouds may have a minimal impact on the
611 derived cloud-free SW flux trends.

612 *4.2.4 Surface Wind and ADMs:* The uncertainty in cloud-free SW flux trends are also examined
613 as a function of surface wind speeds and ADMs. As mentioned previously, the effect of surface
614 wind speed is included in CERES ADMs (used in the SSF data set). Thus, the SWARE trends
615 derived from the CERES SSF datasets are used to investigate ADMs and surface wind speed

616 related uncertainties in this study. Based on Table 3, the cloud-free sky SW flux trends derived
617 from the CERES SSF SW flux are -0.26 and $-1.22 \text{ Wm}^{-2} \text{ decade}^{-1}$ for using Aqua and Terra
618 datasets respectively, and the numbers are -0.50 and $-1.50 \text{ Wm}^{-2} \text{ decade}^{-1}$ for using CERES ES-8
619 data. Thus, the cloud-free SW flux trends derived using the CERES ES-8 are on the order of -
620 $0.25 \text{ Wm}^{-2} \text{ decade}^{-1}$ (corresponding to standard deviation values of 0.20 and $0.17 \text{ Wm}^{-2} \text{ decade}^{-1}$
621 for Terra and Aqua, respectively) lower than the same trends derived using CERES SSF data for
622 the same study period. The $\sim 0.25 \text{ Wm}^{-2} \text{ decade}^{-1}$ difference indeed contains combined
623 uncertainties from ADMs as well as the changes in surface wind speeds for both Terra and Aqua
624 datasets.

625 Overall, the largest sources of uncertainty in the SWARE trend estimates are from ADMs
626 / near surface wind speed changes while the impact of cloud contamination is rather minor. If
627 we assume the standard deviation values from Table 5 can be considered as uncertainties, an
628 overall uncertainty in the trend analysis can be estimated based on equation 4 (Penner et al.,
629 1994; Zhang et al., 2005b):

$$630 \quad U_t = e^{[\sum \log U_i^2]^{0.5}} \quad (4)$$

631
632 Where U_t is the overall uncertainty factor and U_i is the uncertainty factor from each item
633 in Table 5. The uncertainty factor is defined as such that if the percentage uncertainty is 8%,
634 then the uncertainty factor is 1.08. As shown in Table 5, estimated from Equation 4, the overall
635 uncertainties for the SWARE trends estimated using CERES SSF data are 0.3 and 0.2 Wm^{-2}
636 decade^{-1} for Terra and Aqua based analyses respectively, shown also in Table 5. Note that
637 similar numbers are also found by repeating the same exercise but using CERES ES-8 data as
638 shown in Table 5.

5. Comparison to other aerosol related trend analyses

Both AOT and SWARE trends are estimated in this study. Using CALIOP data from 2006-2014, Toth et al. (2016) studied AOT and aerosol vertical distribution trends over both land and oceans. Alfaro-Contreras et al. (2016) explored temporal variations in above cloud AOT with the combined use of Ozone Monitoring Instrument (OMI) and CALIOP data. Although different spectral widths (narrowband versus broadband), different instruments (passive versus active sensors) and different observing conditions (cloud-free skies versus cloudy skies) are considered in different studies, it is interesting to inter-compare trends derived from those studies, as shown in Table 6. Another reason for selecting these studies is because AOT trends for similar regions are reported.

Four studies are listed in Table 6, including passive based AOT analysis (Zhang and Reid 2010; this study); SWARE analysis (this study); CALIOP-based AOT analysis (Toth et al., 2016); and above-cloud AOT analysis (Alfaro-Contreras et al., 2016). It should be noted that only over ocean data are used for the studies utilizing passive-based instruments (Zhang and Reid, 2010; current study). The estimated trends from the active-based studies (Alfaro-Contreras et al., 2016; Toth et al., 2016) included both land and ocean CALIOP data. Also, different data sampling, data screening, and filtering methods are applied for different studies.

Table 6 includes estimates for global oceans for 7 selected regions that have reported values from all four studies. It is interesting to note that positive trends in AOT (both from passive and active methods), SWARE, and above cloud AOT are found over the Bay of Bengal and Arabian Sea, although trends from some analyses are insignificant such as from the above cloud AOT analysis (Alfaro-Contreras et al., 2016). Negative trends are found, across all four studies, over

662 the Mediterranean Sea and eastern coast of the US. The cohesive results from studies using
663 different instruments with varying methods, seem to add more fidelity to the trend analysis of
664 this study.

665 Still, over coastal China, while Zhang and Reid (2010) reported a statistically significant
666 positive AOT trend for the study period of 2000-2009, negative AOT trends are found from both
667 this study (2000-2015) and Toth et al., (2016; for 2006-2014). Again, this is because a potential
668 increase in aerosol loading for the early study period (2000-2007) continued with a decreasing
669 trend in aerosol loading after 2008, as suggested by a recent study (Zhang et al., 2017).

670

671 **6. Summary and Conclusions**

672 Using Terra (2000-2015) and Aqua (2002-2015) Collection 6 (C6) Moderate Resolution and
673 Imaging Spectroradiometer (MODIS) Dark Target (DT), Multi-angle Imaging Spectroradiometer
674 (MISR; 2000-2015) and Cloud and Earth's Radiant Energy System (CERES) ES-8/SSF data,
675 both Aerosol Optical Thickness (AOT) and Short-Wave Aerosol Radiative Effect (SWARE)
676 trends are estimated over global oceans. The results of this study are inter-compared with
677 analyses from several other studies that derived AOT trends using different instruments (e.g,
678 active versus passive) over different observing scenes (e.g. cloudy versus cloud free). This study
679 suggests:

- 680 1. Updating the analysis from Zhang and Reid (2010), which examined AOT trend over
681 global oceans using the Collection 5 (C5) Terra MODIS DT aerosol data for 2000-2009,
682 the use of the newly released C6 Terra MODIS DT aerosol products introduces a
683 marginal differences in derived global and regional AOT trends.

2. Using the near full data record from Terra (2000-2015), Aqua (2002-2015), and MISR (2000-2015), global and regional AOT trends are derived using over ocean C6 MODIS DT and MISR data. A negligible AOT trend ($0.0003 \text{ AOT decade}^{-1}$) is found using Aqua C6 MODIS DT data, but a higher AOT trend of $0.008 \text{ AOT decade}^{-1}$ is found using Terra C6 MODIS DT data, while a slight negative trend is derived using MISR data ($-0.005 \text{ AOT decade}^{-1}$). It is suspected that the difference may be introduced by calibration related issues for one or all sensors, such as the recently reported cross-talk in thermal channels for Terra MODIS (Moeller and Frey, 2016), and a slight decrease in signal sensitivity for Terra MISR (Limbacher and Kahn, 2016). After accounting for potential calibration drifts, negligible AOT trends are found over global oceans using data from all sensors.
3. Regionally, statistically significant increases in aerosol loading over time are found over regions such the Indian Bay of Bengal, Arabian Sea, and the Red Sea. Statistically significant negative AOT trends are also found over the eastern US coast and Mediterranean Sea. This is in agreement from all three sensors (MODIS Aqua, MODIS Terra and MISR).
4. Using collocated MODIS and CERES data over global oceans, the SW flux (*SWARE*) trends are also estimated for the near-full Terra (2000-2015) and Aqua (2002-2015) data records. After accounting for the potential calibration / angular distribution models (ADMs) / near surface wind related issues, small negative (*positive*) trends of -0.5 to $-0.6 \text{ Wm}^{-2} \text{ decade}^{-1}$ ($0.5 - 0.6 \text{ Wm}^{-2} \text{ decade}^{-1}$) are found for Terra based analysis and a near zero trend is found for using Aqua data, and the results are rather consistent regardless of using CERES SSF or ES-8 SW fluxes. Regionally, positive SW flux trends are found

over regions such as the Bay of Bengal and Arabian Sea, where statistically significant negative trends are found over the eastern US coast and Mediterranean Sea. The signs of the regional SW flux trends are in good agreement to what has been found for AOT trends.

5. Very high correlations are found between MODIS DT AOT and CERES cloud-free SW flux values using $2 \times 2^\circ$ (Latitude/Longitude) gridded multi-year mean Terra (2000-2015) and Aqua (2002-2015) data. The SW aerosol direct forcing efficiency is estimated to be -60 Wm^{-2} per AOT and a SWARE value of -7 Wm^{-2} is derived over global oceans. The results are consistent, regardless of using Terra or Aqua data, or using of CERES ES-8 or SSF data. Regionally, over the southwest coast of Africa, where smoke aerosol particles dominate in summer months, a SW aerosol direct forcing efficiency value of $\sim -40 \text{ Wm}^{-2}$ per AOT is found, again, regardless of datasets used. SW aerosol direct forcing efficiency values of -50 to -80 Wm^{-2} per AOT are also found for Arabian Sea, northwest coast of Africa, coastal China and Indian Bay of Bengal, where dust and pollutant aerosols dominate. [It also worth noting that a non-linear relationship is found between SWARE and AOT.](#)

6. Factors that could impact SWARE trend analysis include cloud contamination, calibration drifts, ADMs, ocean wind patterns, and optically thin cirrus (OTC) clouds. The largest sources of uncertainty in the derived SWARE trends are found to be related to ADMs/surface wind speeds, while cloud contamination has a minor impact on the estimated SWARE trends.
7. Finally, trend analyses from this study are inter-compared with results from several selected studies (e.g., Zhang and Reid, 2010; Alfaro-Contreras et al, 2016; Toth et al.,

2016). Consistency in increasing/decreasing AOT trends is found among the studies, using passive and active based instruments, over cloud free and cloudy skies, as well as using narrowband and broadband observations over regions such as the Bay of Bengal, Arabian Sea, the eastern US coast and Mediterranean Sea. Note that the above mentioned studies are derived with different instruments that have different sampling methods with different uncertainties under different observing conditions. The fact that consistencies are found from those studies, adds fidelity to some of the studies that are difficult to evaluate otherwise~~This study suggests that comprehensive observational systems can and should be used in future studies to gain a better understanding of any changes in atmospheric aerosol states.~~

Acknowledgments

Author RC acknowledges the support from a NASA project NNX14AJ13G and a NSF project IIA-1355466. Author J. Zhang also acknowledges the support from an ONR 32 project N00014-16-1-2040 (Grant 11843919). Author JS Reid was supported by ONR 32 project N00014-16-1-2040

References

- Alfaro-Contreras, R., Zhang, J., Campbell, J.R., and Reid, J.S.: Investigating the frequency and interannual variability in global above-cloud aerosol characteristics with CALIOP and OMI, *Atmos. Chem. Phys.*, 16, 47-69, 2016.
- Al Senafi, F., and Anis, A.: Shamals and climate variability in the Northern Arabian/Persian Gulf from 1973-2012, *Int. J. Climo.*, 35, 4509-4528, doi: 10.1002/joc.4302, 2015.
- Barkstrom, B.R., and Wielicki, B.A.: Cloud and the Earth's Radiant Energy System (CERES) Algorithm and Theoretical Basis Document: CERES Data Processing Objectives and Architecture (Subsystem 0), 1996.
- Chin, M., Diehl, T., Tan, Q., Prospero, J. M., Kahn, R. A., Remer, L. A., Yu, H., Sayer, A. M., Bian, H., Geogdzhayev, I. V., Holben, B. N., Howell, S. G., Huebert, B. J., Hsu, N. C., Kim, D., Kucsera, T. L., Levy, R. C., Mishchenko, M. I., Pan, X., Quinn, P. K., Schuster, G. L., Streets, D. G., Strode, S. A., Torres, O., and Zhao, X.-P.: Multi-decadal aerosol variations from 1980 to 2009: a perspective from observations and a global model, *Atmos. Chem. Phys.*, 14, 3657-3690, <https://doi.org/10.5194/acp-14-3657-2014>, 2014.
- Christopher, S. A.: Satellite remote sensing methods for estimating clear Sky shortwave Top of atmosphere fluxes used for aerosol studies over the global oceans, *Remote Sensing of Environment*, doi:10.1016/j.rse.2011.06.003, 2011.
- Christopher, S. A., and Zhang, J.: Daytime variation of shortwave direct radiative forcing of biomass burning aerosols from GOES 8 imager, *J. Atmos. Sci.*, 59(2), 681-691, 2002a.
- Christopher, S. A., and Zhang, J.: Shortwave aerosol radiative forcing from MODIS and CERES observations over the oceans, *Geophys. Res. Lett.*, 29(18), 1859, doi:10.1029/2002GL014803, 2002b.

Formatted: Justified, Line spacing: Double

773 Christopher, S. A., and Jones, T. A.: Short-wave aerosol radiative efficiency over the global
774 oceans derived from satellite data, *Tellus B*, 60, 636–640. doi:10.1111/j.1600-
775 0889.2008.00353.x, 2008.

776 Diner, D.J., Beckert, J.C., Bothwell, G.W., and Rodriguez, J.I.: Performance of the MISR
777 instrument during the first 20 months in Earth orbit, *IEEE T. Geosci. Remote Sens.*,
778 40(7),1449-1466, 2002.

Formatted: Justified, Indent: Left:
0 cm, Hanging: 1.27 cm, Space
After: 0 pt, Line spacing: Double

779 Feng, Q., Hsu, N.C., Yang, P., and Tsay, S.-C.: Effect of thin cirrus cloud on dust optical depth
780 retrievals from MODIS observations, *IEEE Tran. Geosci. Remote Sens.*, 49, No.8, 2011.

Formatted: Font: Not Italic

781 Geier, E. B., Green, R. N., Kratz, D.P., Minnis, P., Miller, W.F, Nolan, S.K., and Franklin, C.B.:
782 Single satellite footprint TOA/surface fluxes and clouds (SSF) collection document, cited
783 2003. [http://ceres.larc.nasa.gov/documents/collect_guide/pdf/SSF_CG_R2V1.pdf].

Formatted: Justified, Indent: Left:
0 cm, Hanging: 1.27 cm, Space
After: 0 pt, Line spacing: Double

784 Huang, J., Hsu, N.C., Tsay, S.C., Jeong, M.-Y., Holben, B.N., Berkoff, T.A., and Ellsworth,
785 J.W.: Susceptibility of aerosol optical thickness retrievals to thin cirrus contamination
786 during the BASE-ASIA campaign, *J. Geophys. Res.* 116, D08214,
787 doi:10.1029/2010JD014910, 2011.

Formatted: Font: Not Italic

788 Hsu, N. C., Gautam, R., Sayer, A. M., Bettenhausen, C., Li, C., Jeong, M. J., Tsay, S.-C., and
789 Holben, B. N.: Global and regional trends of aerosol optical depth over land and ocean
790 using SeaWiFS measurements from 1997 to 2010, *Atmos. Chem. Phys.*, 12, 8037-8053,
791 doi:10.5194/acp-12-8037-2012, 2012.

792 IPCC: Climate Change 2013: The Physical Science Basis: Summary for Policymakers,
793 Cambridge, UK, 2013.

Formatted: Justified, Indent: Left:
0 cm, Hanging: 1.27 cm, Space
After: 0 pt, Line spacing: Double

794 Kaufman, Y. J., Remer, L.A., Tanre, D., Li, R.-R., Kleidman, R., Mattoo, S., Levy, R., Eck, T.,
795 Holben, B.N., Ichoku, C., Martins, V., and Koren, I.: A critical examination of the

Formatted: Font: Not Italic

Formatted: Font: Not Italic

796 [residual cloud contamination and diurnal sampling effects on MODIS estimates of](#)
797 [aerosol over ocean, IEEE Trans. Geosci. Remote Sens., 43, 2886–2897, 2005.](#)

798 Kahn, R. A., Gaitley, B. J., Garay, M. J., Diner, D. J., Eck, T., Smirnov, A., and Holben, B. N.:
799 Multiangle Imaging Spectroradiometer global aerosol product assessment by comparison
800 with Aerosol Robotic Network. J. Geophys. Res., Vol. 115, D23209, doi:
801 10.1029/2010JD014601, 2010.

802 Kato, S., Rose, F.G., Sun-Mack, S., Walter, F.M., Chen, Y., Rutan, D.A., Stephens, G.L., Loeb,
803 N.G., Minnis, P., Wielicki, B.A., Winker, D.M., Charlock, T.P., Stackhouse, P.W., Xu,
804 K.-M., and Collins, W.D.: Improvements of top-of-atmosphere and surface irradiance
805 computations with CALIPSO-, CloudSat-, and MODIS-derived cloud and aerosol
806 properties, J. Geophys. Res., 116, D19209, doi:10.1029/2011JD016050., 2011.

807 Kendall, M.G.: Rank Correlation Methods. Griffin: London, 1975.

808 Klingmüller, K., Pozzer, A., Metzger, S., Stenchikov, G. L., and Lelieveld, J.: Aerosol optical
809 depth trend over the Middle East, Atmos. Chem. Phys., 16, 5063-5073, doi:10.5194/acp-
810 16-5063-2016, 2016.

811 Levy, R.C., Mattoo, S., Munchak, L.A., Remer, L.A., Sayer, A.M., Patadia, F., Hsu, N.C.: The
812 Collection 6 MODIS aerosol products over land and ocean, Atmos. Meas. Tech., 6, 2989-
813 3034, doi:10.5194/amt-6-2989-2013, 2013.

814 Li, J., Carlson, B.E., Dubovik, O., and Lacis, A.A.: Recent trends in aerosol optical properties
815 derived from AERONET measurements, Atmos. Chem. Phys., 14, 12271-12289, doi:
816 10.5194/acp-14-12271-2014, 2014.

Formatted: Font:

817 Loeb, N. G., and Kato, S.: Top-of-atmosphere direct radiative effect of aerosols from the Clouds
818 and the Earth's Radiant Energy System (CERES) satellite instrument, J. Clim. 15, 1474–
819 1484, 2002.

820 Loeb, N. G., Smith, N. M., Kato, S., Miller, W.F., Gupta, S.K., Minnis, P., and Wielicki, B.A.:
821 Angular distribution models for top-of-atmosphere radiative flux estimation from the
822 Clouds and the Earth's Radiant Energy System instrument on the Tropical Rainfall
823 Measuring Mission Satellite. Part I: Methodology. J. Appl. Meteor., 42, 240–266, 2003.

824 Limbacher, J. A., and Kahn R. A.: Updated MISR Dark-Water Research Aerosol Retrieval
825 Algorithm – Part 1: Empirical Calibration Corrections and Coupled 1.1 km Ocean-
826 Surface Chlorophyll-a Retrievals, Atmos. Meas. Tech. Discuss., doi:10.5194/amt-2016-
827 360, in review, 2016.

828 Mann, H.B.: Nonparametric tests against trend. Econometrica 13: 245–259, 1945.

829 Mishchenko, M. I., Liu, L., Geogdzhayev, I. V., Li, J., Carlson, B. E., Lacis, A. A., Cairns, B.,
830 and Travis, L. D.: Aerosol retrievals from channel-1 and -2 AVHRR radiances: Long-
831 term trends updated and revisited, J. Quant. Spectrosc. Ra., 113, 1974–1980, 2012.

832 Moeller C., and Frey R.: Impact of Terra/MODIS PV LWIR cross talk on L1 and L2 Products,
833 The MODIS Science Team Meeting, June 6 – June 10, 2016, Silver Spring, MD, 2016.

834 Penner, J. E., Charlson, R.J., Schwartz, S.E., Hales, J.M., Laulainen, N.S., Travis, L., Leifer, R.,
835 Novakov, T., Ogren, J., and Radke, L.F.: Quantifying and minimizing uncertainty of
836 climate forcing by anthropogenic aerosols, Bull. Am. Meteorol. Soc., 75, 375– 400, 1994.

837

838

Formatted: Justified, Line spacing:
Double

839 Remer L. A., Kaufman Y. J., Tanré D., Mattoo S., Chu D. A., Martins J. V., Li R. R., Ichoku C.,
840 Levy R. C., Kleidman R. G., Eck T. F., Vermote E., and Holben B. N.: The MODIS
841 aerosol algorithm, products, and validation, *J. Atmos. Sci.*, 62, pp. 947–973, doi:
842 <http://dx.doi.org/10.1175/JAS3385.1>, 2005.

843 Remer, L. A., Kaufman, Y. J., and Kleidman, R. G.: Comparison of three years of Terra and
844 Aqua MODIS Aerosol Optical Thickness Over the Global Oceans. *IEEE, Geosci. Remote*
845 *Sens. Lett.*, 3(4), 537–540, 2006.

846 Shi, Y., Zhang, J., Reid, J. S., Holben, B., Hyer, E. J., and Curtis, C.: An analysis of the
847 collection 5 MODIS over-ocean aerosol optical depth product for its implication in
848 aerosol assimilation, *Atmos. Chem. Phys.*, 11, 557–565, doi:10.5194/acp-11-557-2011,
849 2011.

850 Solomon, F., Nair, V. S., and Mallet, M.: Increasing Arabian dust activity and the Indian summer
851 monsoon, *Atmos. Chem. Phys.*, 15, 8051-8064, doi:10.5194/acp-15-8051-2015, 2015.

852 Suttles, J. T., Green, R.N., Minnis, P., and Stowe, L.L.: Angular radiation models for Earth-
853 atmosphere system. I—Shortwave radiation, Rep. NASA RP-1184, 144 pp., NASA,
854 Greenbelt, Md., 1988.

855 Thomas, G. E., Poulsen, C. A., Siddans, R., Sayer, A. M., Carboni, E., Marsh, S. H., Dean, S.
856 M., Grainger, R. G., and Lawrence, B. N.: Validation of the GRAPE single view aerosol
857 retrieval for ATSR-2 and insights into the long term global AOD trend over the ocean,
858 *Atmos. Chem. Phys.*, 10, 4849–4866, doi:10.5194/acp-10-4849-2010, 2010.

859 Toth T.D., Zhang, J., Campbell J.R., Reid, J.S., Shi. Y, Johnson, R.S., Smirnov, A., Vaughan, M.
860 A., and Winker, D.M.: Investigating enhanced Aqua MODIS aerosol optical depth
861 retrievals over the mid-to-high latitude Southern Oceans through intercomparison with

Formatted: Justified, Line spacing:
Double

co-located CALIOP, MAN, and AERONET data set, *J. Geophys. Res. Atmos.*, 118,
4700-4714, doi:10.1002/jgrd.50311, 2013.

Toth, T.D., Zhang, J., Campbell, J.R., Reid, J.S., and Vaughan, M.A.: Temporal variability of
aerosol optical thickness vertical distribution observed from CALIOP, *J. Geophys. Res.*
Atmos., 121, doi:10.1002/2015JD024668, 2016.

Weatherhead, E. C., Reinsel, G. C., Tiao, G. C., Meng, X. L., Choi, D., Cheang, W. K., Keller,
T., DeLuisi, J., Wuebbles, D. J., Kerr, J. B., Miller, A. J., Oltmans, S. J. and Frederick, J.
E.: Factors affecting the detection of trends: statistical considerations and applications to
environmental data, *J. Geophys. Res.*, 103, 17149– 17161, 1998.

Wielicki, B. A., Barkstrom, B.R., Harrison E.F., Lee III, R.B., Smith G.L., and Cooper, J.E.:
Clouds and the Earth's Radiant Energy System (CERES): An Earth Observing System
Experiment, *Bull. Am. Meteorol. Soc.*, 77, 853–868, 1996.

Winker, D. M. and coauthors.: The CALIPSO mission: a global 3D view of aerosols and clouds,
B. Am. Meteorol. Soc., 91, 1211–1229, 2010.

Zhang, J., and Christopher S. A.: Longwave radiative forcing of Saharan dust aerosols from
Terra, *Geophys. Res. Lett.*, 30 , 2188, doi:10.1029/2003GL018479, 2003.

Zhang, J. and Reid, J.S.: MODIS aerosol product analysis for data assimilation: Assessment of
level 2 aerosol optical thickness retrievals, *J. Geophys. Res.*, 111, D22207, doi:10.1029/2005JD006898, 2006.

Zhang J., and Reid, J. S.: An analysis of clear sky and contextual biases using an operational
over ocean MODIS aerosol product, *Geophys. Res. Lett.*, 36, L15824,
doi:10.1029/2009GL038723, 2009.

884 Zhang, J., and Reid, J.S.: A decadal regional and global trend analysis of the aerosol optical
 885 depth using data assimilation grade over-water MODIS and Level 2 MISR aerosol
 886 products, *Atmos. Chem. Phys.*, 10, 10949-10963, doi:10.5194/acp-10-10949-2010, 2010.

887 Zhang, J., Christopher, S.A., Remer, L.A., and Kaufman, Y.J.: Shortwave aerosol radiative
 888 forcing over cloud-free oceans from Terra: 1. Angular models for aerosols, *J. Geophys.*
 889 *Res.*, *D10S23*, doi:10.1029/2004JD005008., 2005a.

890 Zhang, J., Christopher, S.A., Remer, L.A., and Kaufman, Y.J.: Shortwave aerosol radiative
 891 forcing over cloud-free oceans from Terra: 2. Seasonal and global distributions, *J.*
 892 *Geophys. Res.*, *D10S24*, doi:10.1029/2004JD005009, 2005b.

893 Zhang J., Reid, J. S., Alfaro-Contreras, R., and Xian P.: Has China been exporting less air
 894 pollution over the past decade?, *Geophysical Research Letters*, DOI:
 895 10.1002/2017GL072617, 2017.

896 Zhao, X.-P., Chan, P. K., and Heidinger, A. K.: A global survey of the effect of cloud
 897 contamination on the aerosol optical thickness and its long-term trend derived from
 898 operational AVHRR satellite observations, *J. Geophys. Res.*, 118, 2849–2857,
 899 doi:10.1002/jgrd.50278, 2013.

900

Formatted: Justified, Line spacing:
Double

901 Table 1. List of datasets used in the study.

Datasets	Study periods	Purposes
C6 Aqua MODIS DT	July 2002- Dec. 2015	AOT trend, cloud fraction
C6 Terra MODIS DT	Mar. 2000 - Dec. 2015	AOT trend, cloud fraction
Terra MISR	Mar. 2000 - Dec. 2015	AOT trend
C6 Aqua CERES-ES-8-SSF	July 2002 - Dec. 2015	Cloud free SW flux trend
C6 Terra CERES-ES-8-SSF	Mar. 2000 - Dec. 2015	Cloud free SW flux trend
CALIOP	June 2006 - Nov. 2015	Thin cirrus cloud mask

902 Table 2. AOT trend analysis for global and selected regions as suggested from Zhang and Reid, 2010. Both trends from Collection 5
903 (C5, Zhang and Reid, 2010) and Collection 6 (C6) over-water Terra MODIS AOT data are shown for the study period of 2000-2009.
904 The trend significances are derived using two different methods ($|\omega/\sigma_\omega|$ and $|z|$ values as estimated from the Weatherhead and Mann-
905 Kendall methods, respectively). The corrected slopes refer to the slopes after accounting for the slope changes over the Remote Ocean
906 region. AOT trend and trend significances for C5 MODIS DT data are obtained from Zhang and Reid, (2010), which are derived
907 using Data-assimilation Quality C5 MODIS DT data. For illustration purposes, C5* and C6 Terra MODIS AOT values, derived using
908 similar methods as mentioned in this study, are also listed. C5* MODIS DT AOTs listed here are not from the Data-assimilation
909 quality products as used in Zhang and Reid (2010).

Region	Latitude	Longitude	Slope AOT / decade Terra	Trend Significance (Terra)	Corrected Slope AOT/decade (Terra)	Mean AOT (Terra)
--------	----------	-----------	--------------------------------	-------------------------------	---	---------------------

910

			C5	C6	C5 ω/σ_ω	C6 ω/σ_ω	C6 Z	C5	C6	C5*	C6
Global			0.010	0.011	3.60	4.85	6.88	0.003	0.005	0.154	0.140
Africa (NW Coast)	8°N - 24°N	60°W - 18°W	-0.006	-0.004	0.61	0.37	0.18	-0.013	-0.010	0.247	0.257
Bay of Bengal	10°N - 25°N	78°E - 103°E	0.076	0.074	5.63	4.79	4.71	0.069	0.068	0.319	0.326
Coastal China	20°N - 40°N	110°E - 125°E	0.069	0.086	4.06	4.69	4.78	0.062	0.080	0.460	0.462
Central America	5°N - 20°N	120°W - 90°W	-0.016	-0.011	1.73	1.12	0.57	-0.023	-0.017	0.151	0.165
Arabian Sea	5°N - 23°N	50°E - 78°E	0.065	0.077	5.40	4.95	4.03	0.058	0.071	0.319	0.329
Mediterranean Sea	30°N - 45°N	0° - 40° E	-0.009	-0.009	0.94	0.96	1.25	-0.016	-0.015	0.200	0.210
Africa (SW. Coast)	23°S - 7°S	20°W - 15°E	0.016	0.018	1.35	1.52	1.46	0.009	0.012	0.179	0.188
N. America	30°N - 45°N	80°W - 60°W	-0.008	-0.010	1.07	1.50	1.04	-0.015	-0.016	0.157	0.160
Regional (E. Coast)	Lat.	Lon.	AOT decade ⁻¹			Corrected AOT / decade		Cloud-Free Flux wm ⁻² decade ⁻¹		Corrected Cloud-Free Flux wm ⁻² decade ⁻¹	
Africa (SE. coast)	27° - 15°S	32°E - 45°E	0.017	0.015	2.12	1.93	3.06	0.010	0.009	0.129	0.158
Southeast Asia	15°S - 10°N	80°E - 120°E	0.014	0.016	0.80	0.86	4.89	0.007	0.010	0.176	0.184
Remote Ocean	40°S - 0°	179°W - 140°W	0.007	0.006	N/A	2.32	2.93	0	0	0.100	0.107
			MODIS Aqua	MODIS Terra	MISR N/A	MODIS Aqua	MODIS Terra	FS-8 Aqua	FS-8 Terra	FS-8 Aqua	FS-8 Terra

911

912

913 Table 3. Multi-year AOT and Cloud-Free Flux trends (2002-2015 for MODIS Aqua; 2000-2015 for MODIS Terra; and 2000-2015 for
914 MISR) for global and selected regions. AOT trends are calculated using monthly-averaged, deseasonalized AOTs derived from the
915 MODIS collection 6 and MISR aerosol products. Cloud-free flux trends are calculated using seasonally-averaged, deseasonalized
916 cloud-free fluxes derived using the collocated MODIS-CERES SSF/ES-8 data set. Various filtering criteria are applied to the data and
917 described in the text. Trends that are statistically significant with a confidence interval of 95% (utilizing the Weatherhead method for
918 monthly-averages, and the Mann-Kendall method for seasonal-averages) are highlighted in bold.

						Aqua	Terra		SSF	SSF	SSF	SSF
Global			0.0003	0.008	-0.005	~0	0.002	-0.001	-0.50 -0.26	-1.50 -1.22	0 -0.01	-0.58 -0.52
Africa (NW Coast)	8°N - 24°N	60°W - 18°W	0.002	0.009	-0.008	0.002	0.003	-0.004	0.56 0.71	-1.79 -1.29	1.06 0.96	-0.87 -0.59
Bay of Bengal	10°N – 25°N	78°E – 103°E	0.031	0.056	0.018	0.031	0.050	0.022	2.28 1.91	0.79 0.75	2.78 2.16	1.71 1.45
Coastal China	20°N – 40°N	110°E – 125°E	-0.035	0.007	-0.014	-0.035	0.001	-0.01	-0.42 0.04	-2.51 -2.09	0.08 0.29	-1.59 -1.39
Central America	5°N – 20°N	120°W – 90°W	0.007	0.002	-0.011	0.007	-0.004	-0.007	-0.45 -0.11	-1.85 -1.33	0.05 0.14	-0.93 -0.63
Arabian Sea	5°N – 23°N	50°E – 78°E	0.039	0.057	0.033	0.039	0.051	0.037	2.61 2.24	0.90 0.94	3.11 2.49	1.82 1.64
Mediterranean Sea	30°N – 45°N	0° - 40° E	-0.025	-0.014	-0.029	-0.025	-0.020	-0.025	-0.91 -0.72	-2.93 -2.46	-0.41 -0.47	-2.01 -1.76
Africa (SW Coast)	23°S – 7°S	20°W – 15°E	0.016	0.025	0.002	0.016	0.019	0.006	-0.19 0.13	-0.85 -0.57	0.31 0.38	0.07 0.13
East Coast North America	30°N – 45°N	80°W – 60° W	-0.028	-0.016	-0.026	-0.028	-0.022	-0.022	-2.29 -1.65	-3.57 -2.73	-1.79 -1.40	-2.65 -2.03
Africa (SE Coast)	27° - 15°S	32°E - 45°E	0.010	0.017	-0.0001	0.010	0.011	0.004	-0.01 -0.25	-1.46 -1.27	0.49 0	-0.54 -0.57
S.E. Asia	15°S - 10°N	80°E - 120°E	0.013	0.020	0.004	0.013	0.014	0.008	0.02 0.60	-1.07 -0.32	0.52 0.85	-0.15 0.38
Remote Ocean	40°S – 0°	179°W – 140°W	0.0003	0.006	-0.004	0	0	0	-0.50 -0.25	-0.92 -0.70	0 0	0 0
Red Sea	15°N – 30°N	30°E – 45°E	0.081	0.100	0.041	0.081	0.094	0.045	2.52 2.08	-0.27 -0.60	3.02 2.33	0.65 0.1
Persian Gulf	24°N – 30°N	50°E – 60°E	0.033	0.081	0.046	0.033	0.075	0.050	1.76 1.16	-0.64 -0.92	2.26 1.41	0.28 -0.22

920 Table 4. Instantaneous SW aerosol direct forcing efficiencies estimated based on the multi-year means (2000-2015 for Terra and
921 2002-2015 for Aqua) as well as for Dec.-May and Jun.-Nov. seasons using both CERES SSF and ES-8 datasets. Forcing efficiencies
922 are calculated for selected regions that have the maximum 2x2° (Latitude/Longitude) bin-averaged AOT > 0.3, as well as for global
923 oceans. The multi-year mean AOT and SWARE values are estimated using data from all valid bins. Note that values from this table
924 are estimated under CERES cloud free (less 1% cloud fraction, and 99% CP) skies and thus regional and global AOT values may be
925 different from the estimates as shown in Table 2.

	Dec.-May (Wm ⁻² /AOT)		Jun.-Nov. (Wm ⁻² /AOT)		Multi-year Mean (Wm ⁻² /AOT)		Multi-year Mean AOT (0.55 μm)		Multi-year Mean SWARE (Wm ⁻²)	
	Aqua	Terra	Aqua	Terra	Aqua	Terra	Aqua	Terra	Aqua	Terra
	SSF / ES-8	SSF / ES-8	SSF / ES-8	SSF / ES-8	SSF / ES-8	SSF / ES-8	SSF / ES-8	SSF / ES-8	SSF / ES-8	SSF / ES-8
Africa (NW Coast)	-54.1/ -67.0	-52.7/ -63.0	-59.5/ -75.2	-61.1/ -75.9	-54.4 / -65.9	-54.3 / -62.9	0.189 / 0.189	0.204 / 0.204	-10.3 / -12.5	-11.1 / -12.8
Africa (SW Coast)	N/A/ N/A	N/A/ N/A	-40.6/ -44.3	-43.0/ -45.0	-37.8 / -39.8	-42.5 / -43.7	0.160 / 0.160	0.158 / 0.158	-6.0 / -6.4	-6.7 / -6.9
Coastal China	-88.3/ -83.8	-84.0/ -82.4	-74.7/ -74.5	-70.8/ -74.4	-79.0 / -79.5	-74.3 / -79.7	0.293 / 0.293	0.356 / 0.356	-23.2 / -23.3	-26.5 / -28.4
Arabian Sea	-62.0/ -75.3	-66.0/ -75.0	-60.0/ -76.0	-60.6/ -76.5	-61.6 / -76.0	-65.2 / -77.4	0.215 / 0.215	0.238 / 0.238	-13.3 / -16.4	-15.5 / -18.4
Bay of Bengal	-66.4/ -69.3	-52.8/ -63.3	-68.4/ -74.8	-58.4/ -67.8	-74.8 / -80.0	-52.3 / -63.1	0.261 / 0.261	0.295 / 0.295	-19.5 / -20.9	-15.4 / -18.6
Global Oceans	-58.7/ -57.9	-57.3/ -59.4	-56.5/ -59.4	-53.7/ -57.2	-60.9 / -57.7	-57.5 / -58.2	0.116 / 0.116	0.116 / 0.116	-7.1 / -6.7	-6.7 / -6.8

926

927

928

929 Table. 5 List of uncertainty sources (in $\text{Wm}^{-2} \text{decade}^{-1}$) for the estimated cloud-free SW flux trends.

Region / Sensitivity Test	ES-8/SSF Cloud-free flux trends ($\text{Wm}^{-2} \text{decade}^{-1}$)		Standard Deviation ($\text{Wm}^{-2} \text{decade}^{-1}$)	
	Terra ES-8/SSF	Aqua ES-8/SSF	Terra ES-8/SSF	Aqua ES-8/SSF
Global Oceans / No Data Trim	-1.50/-1.22	-0.50/-0.26	0.09/0.08	0.08/0.03
Remote Ocean / No Data Trim				
R.O. Region Outline				
Lat : 40°S - 0° Lon: 180°W - 140°W	-0.92/-0.70	-0.50/-0.25		
Lat: 40°S - 0° Lon: 170°E - 150°W	-1.00/-0.79	-0.47/-0.23		
Lat: 40°S - 0° Lon: 170°W – 130°W	-0.84/-0.63	-0.43/-0.20		
Lat : 50°S – 10°S Lon: 180°W - 140°W	-0.89/-0.67	-0.43/-0.25		
Lat : 30°S - 10°N Lon: 180°W - 140°W	-1.08/-0.81	-0.62/-0.29		
Global Ocean / Variation of CF %			0.04/0.03	0.03/0.01
0 <0.5 <1 <2 <3 <4 <5	-1.46 -1.49 -1.50 -1.51 -1.54 -1.56 -1.57	-0.46 -0.51 -0.52 -0.54 -0.54 -0.55 -0.55		
	-1.22 -1.24 -1.24 -1.25 -1.27 -1.29 -1.30	-0.24 -0.28 -0.28 -0.28 -0.27 -0.26 -0.26		
Global Ocean / Variation of CP %			0.02/0.08	0.01/0.05
100 >99 >98 >97 >96 >95	-1.44 -1.48 -1.49 -1.49 -1.49 -1.49	-0.54 -0.55 -0.54 -0.53 -0.52 -0.52		
	-1.13 -1.26 -1.30 -1.32 -1.34 -1.35	-0.29 -0.23 -0.20 -0.17 -0.16 -0.15		
Global Ocean / Cirrus Contamination			0.08/0.05	0.08/0.05
MODIS-CERES-CALIOP		-0.59/-0.33		
MODIS-CERES-CALIOP (cirrus filtered)		-0.48/-0.26		
ADMs / Wind Speeds			0.20/0.20	0.17/0.17
Global Full Data Record (ES-8)	-1.50	-0.50		
Global Full Data Record (SSF)	-1.22	-0.26		
Overall Uncertainty			0.3/0.3 $\text{Wm}^{-2}/$ decade	0.2/0.2 $\text{Wm}^{-2}/$ decade

931 Table 6. Inter-comparison of AOT (AOT decade^{-1}) and SW flux ($\text{Wm}^{-2} \text{decade}^{-1}$) trends from this study as well as a few previous

	Zhang and Reid (2010) Terra MODIS C5 March 2000- Dec. 2009		This Study Terra MODIS C6 March 2000 – Dec. 2015				Toth et al., 2016 Aqua CALIOP Cloud-Free June 2006 – Dec. 2014	Alfaro-Contreras et al., 2016 Aqua CALIOP Above-Cloud June 2006 – Dec. 2014
Region	$\Delta\text{AOT} / \text{Decade}$		$\Delta\text{AOT} / \text{Decade}$		$\Delta \text{Cloud-Free Flux}$ $\text{Wm}^{-2} \text{decade}^{-1}$ (ES-8/SSF)		$\Delta\text{AOT} / \text{Decade}$	$\Delta\text{AOT} / \text{Decade}$
	w/o correction	w/ correction	w/o correction	w/ correction	w/o correction	w/ correction		
Global Ocean	0.010	0.003	0.008	0.002	-1.50/-1.22	-0.58/-0.52	0.002	0.005
Africa (NW Coast)	-0.006	-0.013	0.009	0.003	-1.79/-1.29	-0.87/-0.59	-0.014	0.0007
Bay of Bengal	0.076	0.069	0.056	0.050	0.79/0.75	1.71/1.45	0.016	0.079
Coastal China	0.069	0.062	0.007	0.001	-2.51/-2.09	-1.59/-1.39	-0.017	0.01
Arabian Sea	0.065	0.058	0.057	0.051	0.90/0.94	1.82/1.64	0.027	0.055
Med. Sea	-0.009	-0.016	-0.014	-0.020	-2.93/-2.46	-2.01/-1.76	-0.006	-0.010
Africa (SW Coast)	0.016	0.007	0.025	0.019	-0.85/-0.57	0.07/0.13	0.009	0.007
N. America (East Coast)	-0.008	-0.015	-0.016	-0.022	-3.57/-2.73	-2.65/-2.03	-0.013	-0.02
Remote Ocean	0.007	0	0.006	0	-0.92/-0.70	0/0		0.005

932 studies at both regional and global scales.

Figure Captions

Figure 1. Spatial distribution of trends for (a) over ocean Terra MODIS DT AOT for 2000-2009, (b) over ocean Terra MODIS DT AOT for 2000-2015, (c) over ocean Aqua MODIS DT AOT for 2002-2015 and (d) over land and ocean Terra MISR AOT for 2000-2015 for every $1^\circ \times 1^\circ$ bin. (e) Ratios of MODIS C6 to C5 AOT trends for the study period of 2000-2009, and (f) Differences in MODIS C6 to C5 AOT trends for the study period of 2000-2009. Regions with statistically significant trends at a confidence interval of 95% are highlighted with black dots. Figs. 1e and 1f are constructed with the use of grids with AOT trends above or below ± 0.0002 AOT/year.

Figure 2. (a) The global distribution of daytime AOTs constructed using sixteen years (2000-2015) of monthly-averaged over ocean C6 Terra MODIS AOTs at a $1^\circ \times 1^\circ$ resolution. Only those bins with more than one thousand data counts were considered for this analysis. (b) Similar to Fig. 2a, but using over ocean C6 Aqua MODIS AOTs for the study period of 2002-2015. (c) Similar to Fig. 2a, but using both over ocean and over land Terra MISR AOT data for the study period of 2000-2015. (d) Differences in gridded AOTs between Terra MODIS and Terra MISR. (e) The ratios of gridded AOTs between Terra MODIS and Terra MISR.

Figure 3. (a) Monthly-averaged global AOTs derived using operational MODIS C6 aerosol products for Aqua (red), Terra (blue) and MISR (green). Straight lines are the linear fits for the monthly data. (b) Similar to Fig. 3a, but for the deseasonalized, monthly-averaged AOTs. (c) Similar to Fig. 3b, but for the Remote Ocean region as described in Table 3.

956 **Figure 4.** The deseasonalized, monthly and regionally averaged AOTs for eight selected regions
957 utilizing operational MODIS C6 and MISR aerosol products. Straight lines are linear fits to the
958 monthly data.

959
960 **Figure 5.** (a) The spatial distribution of seasonally-averaged AOTs using Terra MODIS DT
961 AOT data from the collocated Terra MODIS-CERES dataset for the study period of 2000-2015,
962 at a spatial resolution of $2 \times 2^\circ$ (Latitude/Longitude). (b) Similar to Figure 5a but using the
963 collocated Aqua MODIS-CERES dataset for the study period of 2002-2015. (c) Seasonally
964 averaged CERES ES-8 cloud-free SW flux constructed using the collocated Terra MODIS-
965 CERES dataset for the study period of 2000-2015. (d) Similar to Figure 5c, but using the
966 collocated Aqua MODIS-CERES dataset for the study period of 2002-2015. (e-f) Similar to
967 Figs 5c and 5d but for the seasonally-averaged CERES SSF cloud-free SW fluxes. (g)
968 Difference between cloud-free SW flux from Figure 5e and 5c. (h) Similar to Fig. 5g, but for
969 Aqua. (i) Collocated Terra MODIS-CERES data counts for every $2^\circ \times 2^\circ$ (Latitude/Longitude)
970 bin. (j) Similar to Fig. 5i, but for Aqua.

971
972 **Figure 6.** (a) Scatter plot of Aqua MODIS AOT versus CERES SSF SW flux (at a $2 \times 2^\circ$
973 resolution) using data as shown in Fig. 5. [Color lines are for selected regions and the black thick](#)
974 [line is for global oceans.](#) (b) Similar to Fig. 6a, but for 5 selected regions that have a maximum
975 AOT > 0.3 as indicated from Fig. 5. (c) Similar to Fig. 6a, but for Terra. (d) Similar to Fig. 6b,
976 but for Terra.

977

978 **Figure 7.** Similar to Fig. 6, but for using collocated MODIS and CERES ES-8 cloud-free SW
979 flux data.

980

981

982 **Figure 8.** (a) Time series of seasonally-averaged, deseasonalized cloud-free SW fluxes over
983 global oceans utilizing the collocated MODIS-CERES (SSF/ES-8) datasets for Terra (green) and
984 Aqua (red). (b) Similar to Fig. 8a but using data from the Remote Ocean region. The ES-8 SW
985 fluxes are depicted by solid lines where SSF SW fluxes are depicted by dashed lines.

986

987 **Figure 9.** Time series of all-sky SW flux over the entire globe (land and ocean). The trends are
988 calculated from monthly-globally averaged all-sky SW fluxes derived from the CERES SSF /
989 ES-8 data. SW fluxes from all scenes including cloudy, clean, land and ocean are taken into
990 account when calculating the monthly averages, which are gridded into a similar resolution as
991 the collocated MODIS-CERES dataset ($2 \times 2^\circ$).

992

993 **Figure 10.** The temporal variations of deseasonalized, seasonally- and regionally- averaged
994 CERES SSF / ES-8 cloud-free fluxes (seasonal anomaly) for 8 selected regions, constructed
995 using the collocated Aqua and Terra MODIS-CERES datasets. The blue lines represent the
996 Terra-based analysis while the red lines represent the Aqua-based analysis and the solid lines
997 represent the ES-8 SW fluxes where the SSF SW fluxes are depicted by dashed lines.

998

Figure 11. The de-seasonalized, seasonally averaged cloud-free fluxes over the Coastal China region derived utilizing the collocated MODIS-CERES (SSF / ES-8) datasets. Straight lines show piecewise linear fits for the study periods of 2000–2008 and 2009–2015.

Figure 12. Spatial distribution of gridded AOT trends for (a) 16 year Terra (2000-2015) and (b) 14 year Aqua (2002-2015) for every 4 x 4° (Latitude/Longitude) bin derived from the collocated MODIS-CERES dataset. AOT trends are constructed using seasonally-averaged AOTs. (c) Spatial distribution of cloud-free-sky CERES ES-8 SW flux trends estimated using the collocated Terra MODIS-CERES data for the study period of 2000-2015. (d) Similar to Figure 12c, but using the collocated Aqua MODIS-CERES (ES-8) dataset for the study period of 2002-2015. (e-f) Similar to Figs. 12c and 12d, but for using CERES SSF data. Grids with statistically significant AOT/clear-sky SW flux trends at the 95 % confidence interval are shown in black dots.

Figure 13. Global AOT trends derived from the (red) MODIS-CERES dataset, (green) MODIS-CERES-CALIOP dataset and (blue) MODIS-CERES-CALIOP dataset after filtering for cirrus clouds. Both CERES SSF and ES-8 data are included. Time series have been derived utilizing seasonal AOT averages. CALIOP is used to locate and remove CERES observations contaminated with cirrus clouds. (b) Depicts the same thing as Fig. 13a, except for the cloud-free flux. This analysis is carried out for the Aqua-based study only.

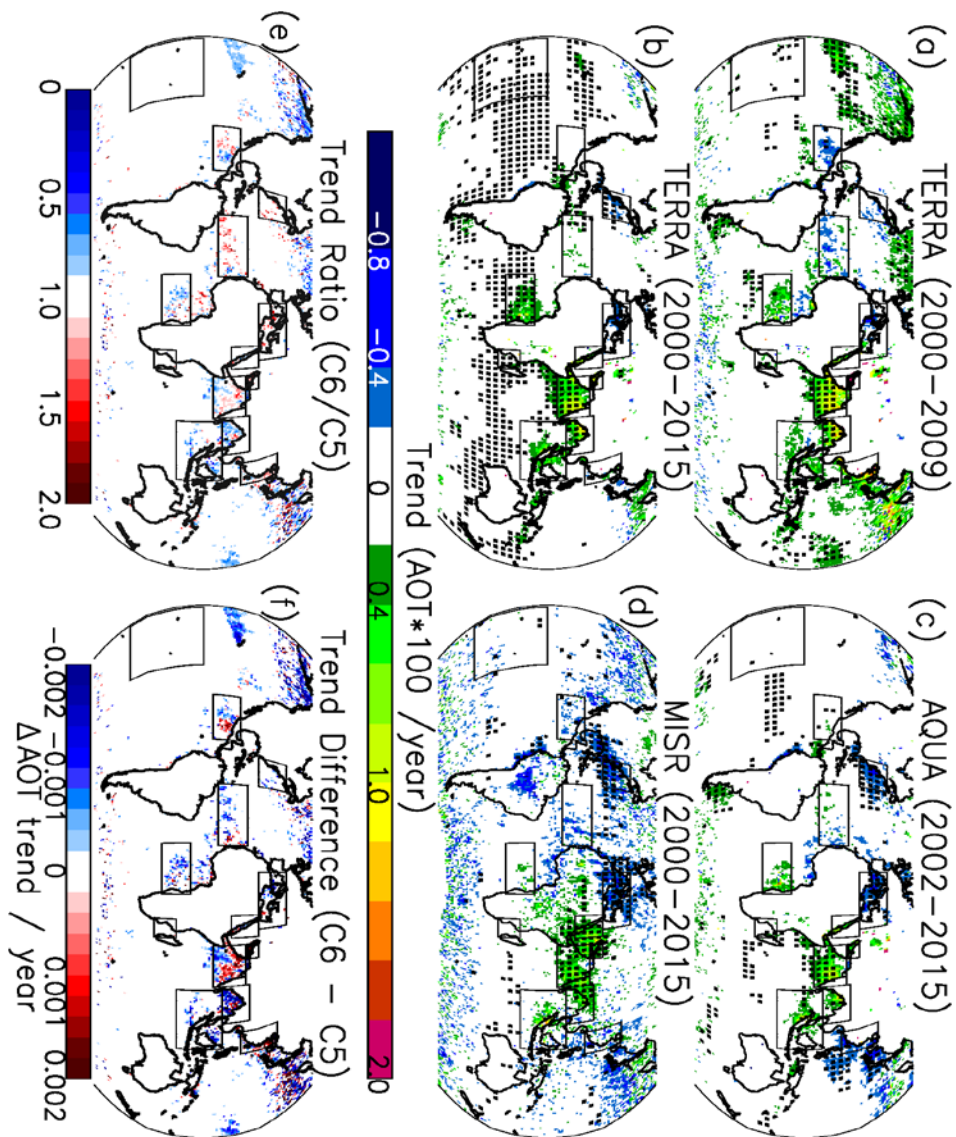
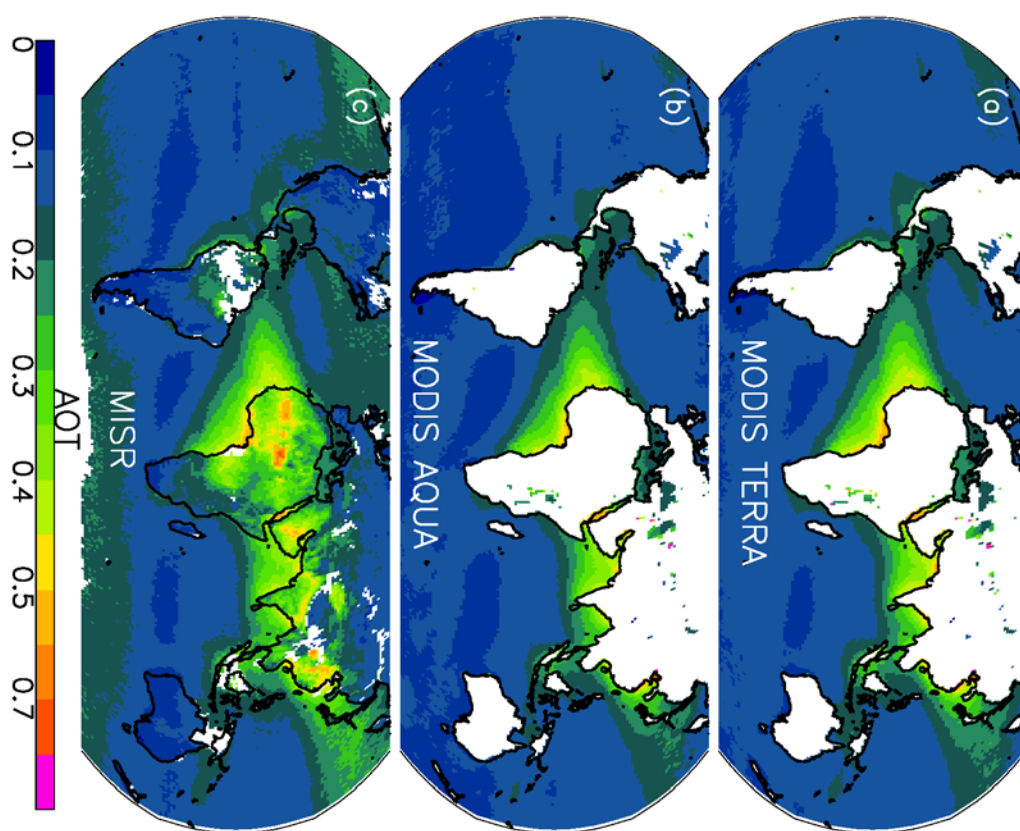


Figure 1. Spatial distribution of trends for (a) over ocean Terra MODIS DT AOT for 2000-2009, (b) over ocean Terra MODIS DT AOT for 2000-2015, (c) over ocean Aqua MODIS DT AOT for 2002-2015 and (d) over land and ocean Terra MISR AOT for 2000-2015 for every $1^\circ \times 1^\circ$ bin. (e) Ratios of MODIS C6 to C5 AOT trends for the study period of 2000-2009, and (f) Differences in MODIS C6 to C5 AOT trends for the study period of 2000-2009. Regions with statistically significant trends at a confidence interval of 95% are highlighted with black dots.

1028 Figs. 1e and 1f are constructed with the use of grids with AOT trends above or below ± 0.0002
 1029 AOT/year.



1030
 1031

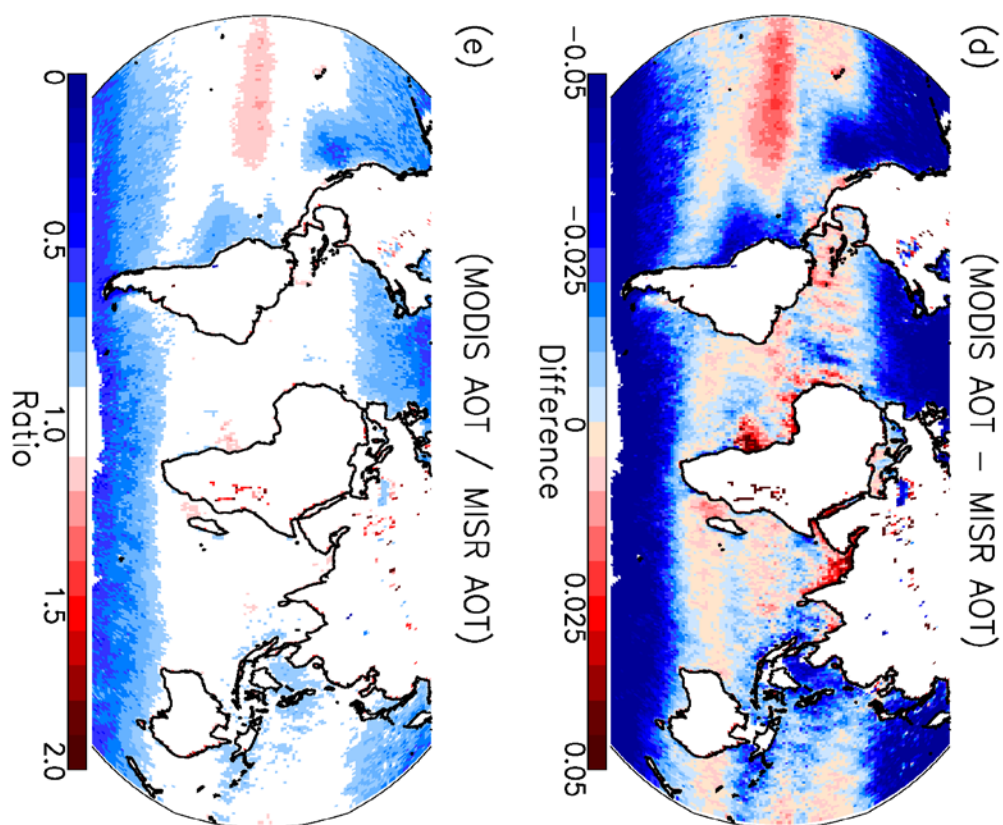
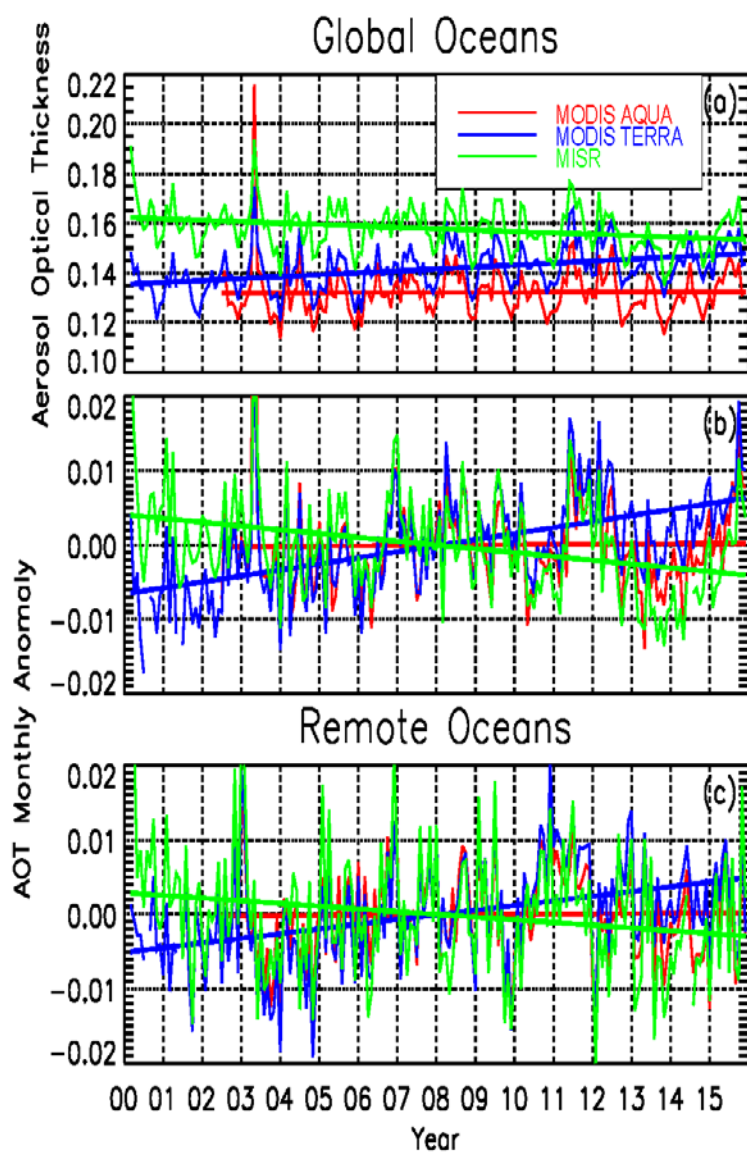


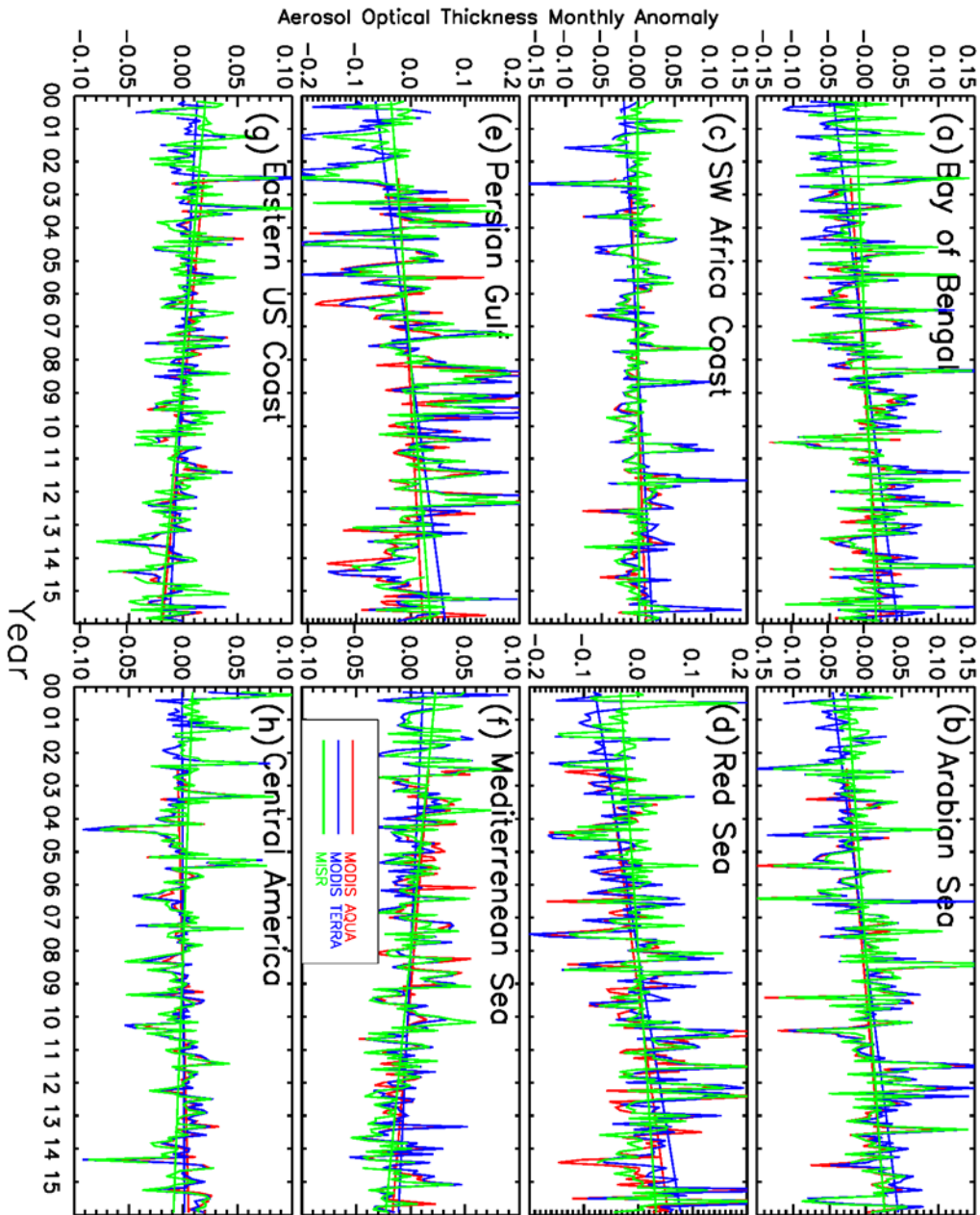
Figure 2. (a) The global distribution of daytime AOTs constructed using sixteen years (2000-2015) of monthly-averaged over ocean C6 Terra MODIS AOTs at a $1^\circ \times 1^\circ$ resolution. Only those bins with more than one thousand data counts were considered for this analysis. (b) Similar to Fig. 2a, but using over ocean C6 Aqua MODIS AOTs for the study period of 2002-2015. (c) Similar to Fig. 2a, but using both over ocean and over land Terra MISR AOT data for the study

1039 period of 2000-2015. (d) Differences in gridded AOTs between Terra MODIS and Terra MISR.
 1040 (e) The ratios of gridded AOTs between Terra MODIS and Terra MISR.

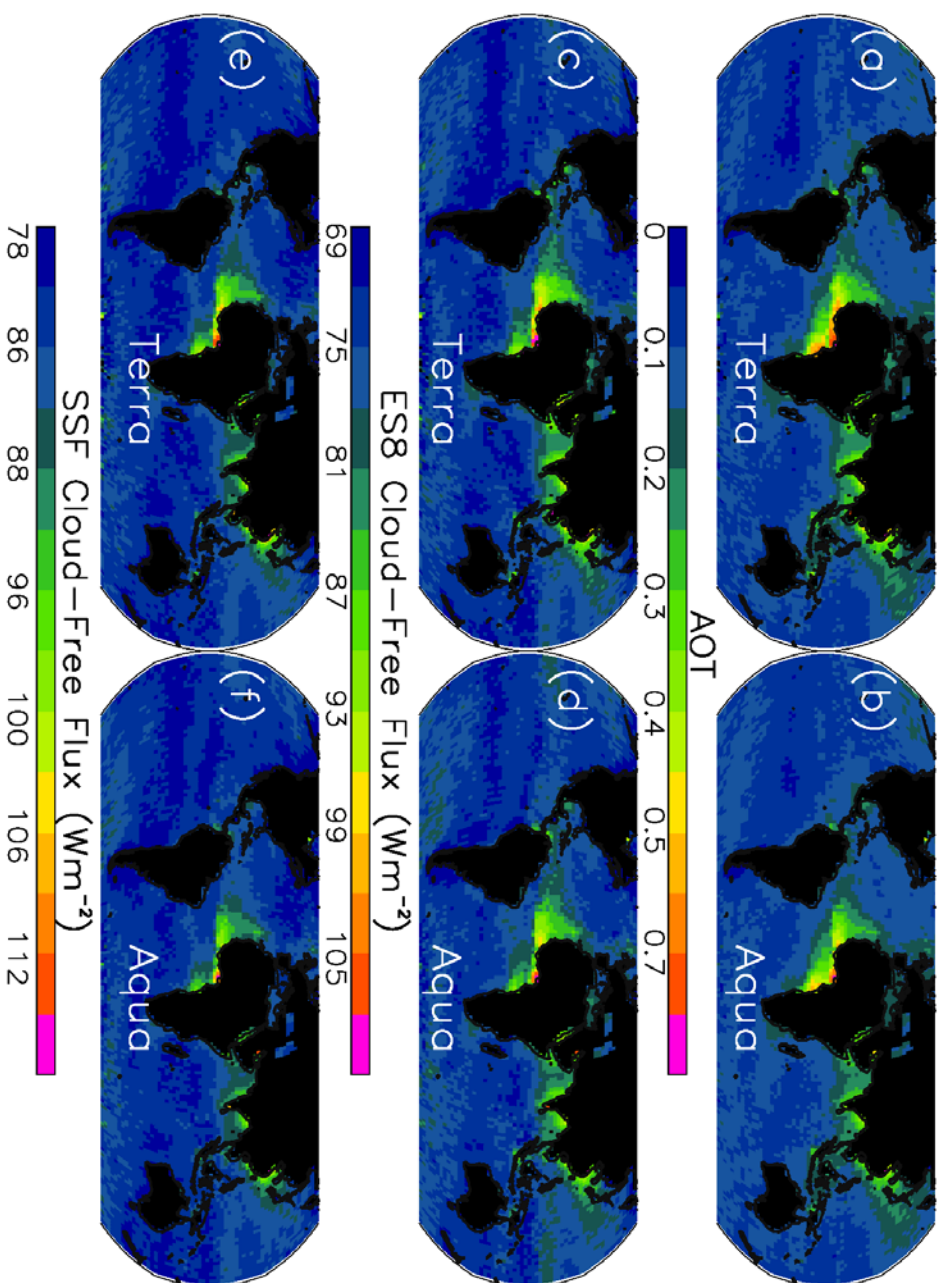


1041
 1042
 1043 **Figure 3.** (a) Monthly-averaged global AOTs derived using operational MODIS C6 aerosol
 1044 products for Aqua (red), Terra (blue) and MISR (green). Straight lines are the linear fits for the

1045 monthly data. (b) Similar to Fig. 3a, but for the deseasonalized, monthly-averaged AOTs. (c)
 1046 Similar to Fig. 3b, but for the Remote Ocean region as described in Table 3.
 1047



1049 **Figure 4.** The deseasonalized, monthly and regionally averaged AOTs for eight selected regions
1050 utilizing operational MODIS C6 and MISR aerosol products. Straight lines are linear fits to the
1051 monthly data.



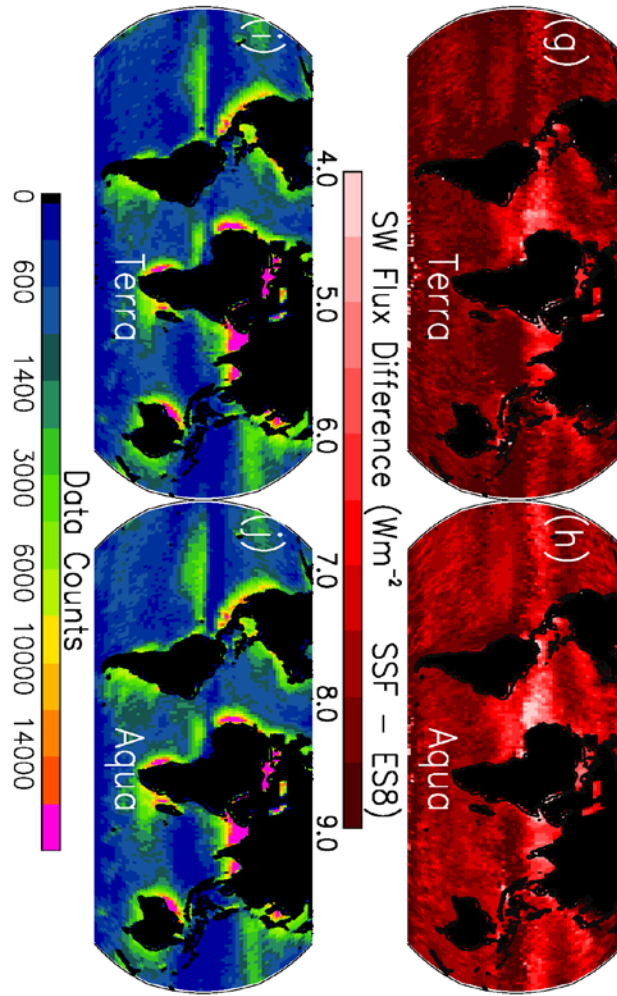
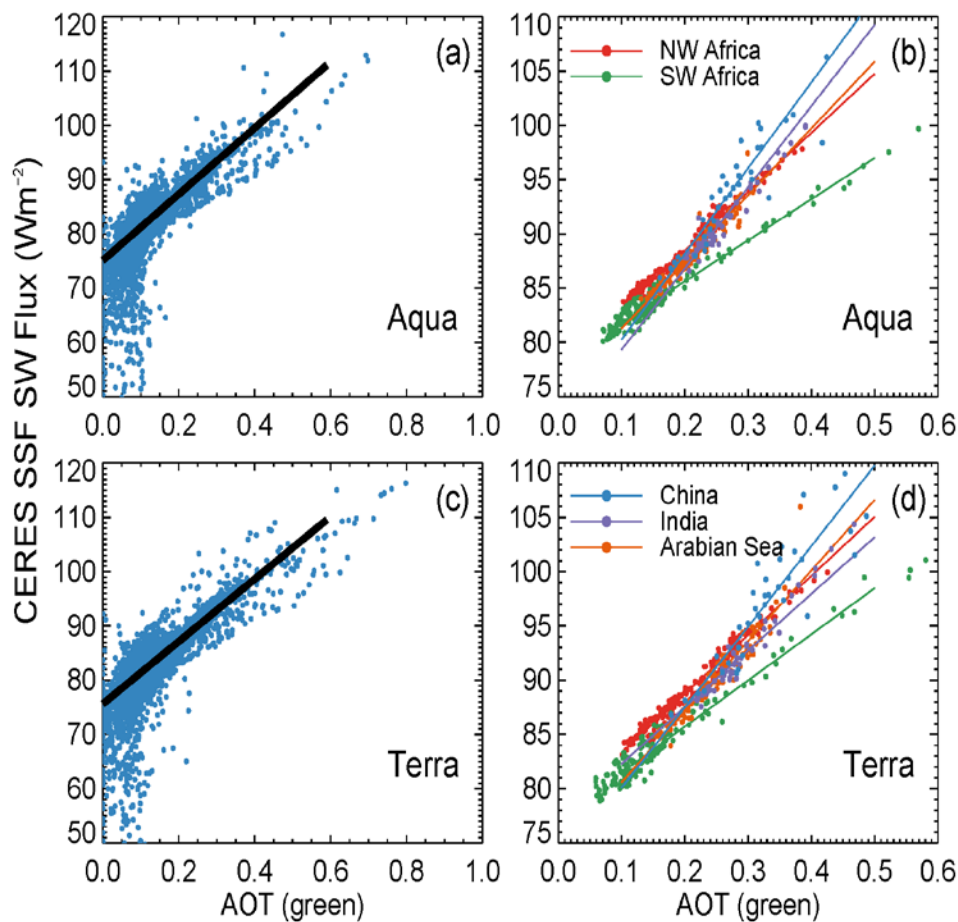


Figure 5. (a) The spatial distribution of seasonally-averaged AOTs using Terra MODIS DT AOT data from the collocated Terra MODIS-CERES dataset for the study period of 2000-2015, at a spatial resolution of $2 \times 2^\circ$ (Latitude/Longitude). (b) Similar to Figure 5a but using the collocated Aqua MODIS-CERES dataset for the study period of 2002-2015. (c) Seasonally averaged CERES ES-8 cloud-free SW flux constructed using the collocated Terra MODIS-CERES dataset for the study period of 2000-2015. (d) Similar to Figure 5c, but using the collocated Aqua MODIS-CERES dataset for the study period of 2002-2015. (e-f) Similar to Figs 5c and 5d but for the seasonally-averaged CERES SSF cloud-free SW fluxes. (g) Difference between cloud-free SW flux from Figure 5e and 5c. (h) Similar to Fig. 5g, but for

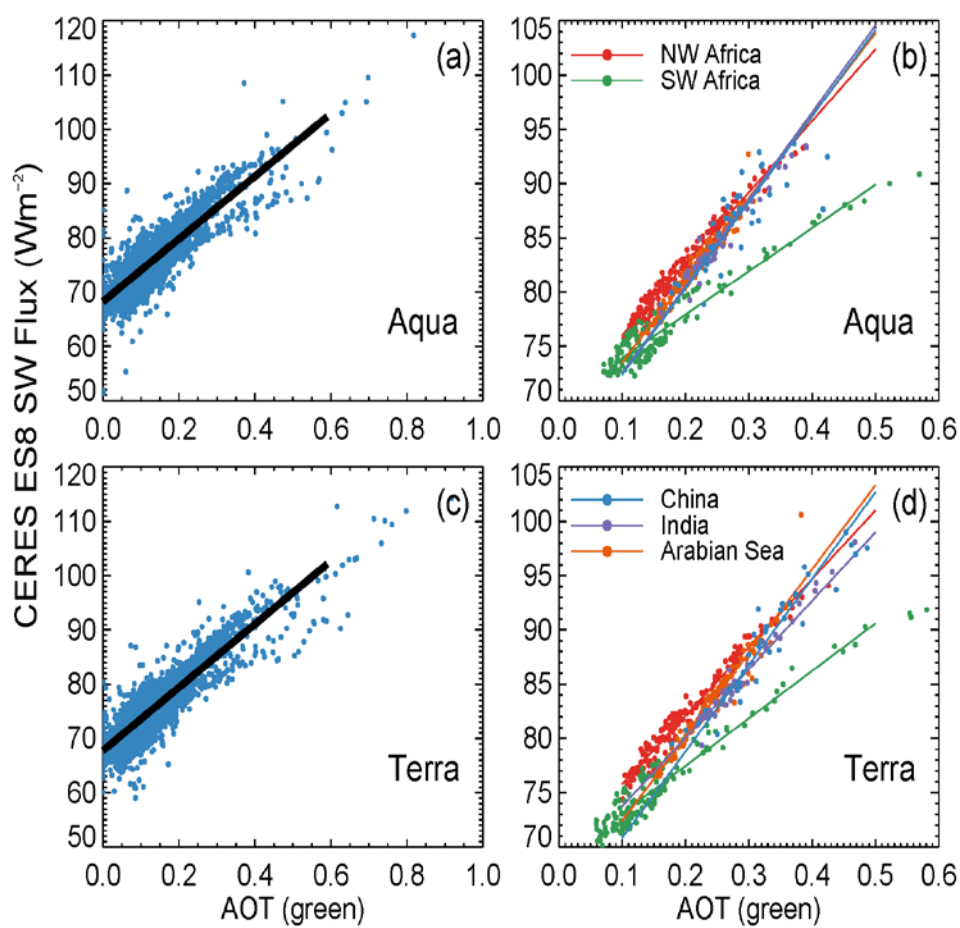
1063 Aqua. (i) Collocated Terra MODIS-CERES data counts for every $2^\circ \times 2^\circ$ (Latitude/Longitude)
 1064 bin. (j) Similar to Fig. 5i, but for Aqua.



1065 **Figure 6.** (a) Scatter plot of Aqua MODIS AOT versus CERES SSF SW flux (at a $2 \times 2^\circ$
 1066 resolution) using data as shown in Fig. 5. Color lines are for selected regions and the black thick
 1067 line is for global oceans. (b) Similar to Fig. 6a, but for 5 selected regions that have a maximum
 1068 AOT > 0.3 as indicated from Fig. 5. (c) Similar to Fig. 6a, but for Terra. (d) Similar to Fig. 6b,
 1069 but for Terra.
 1070

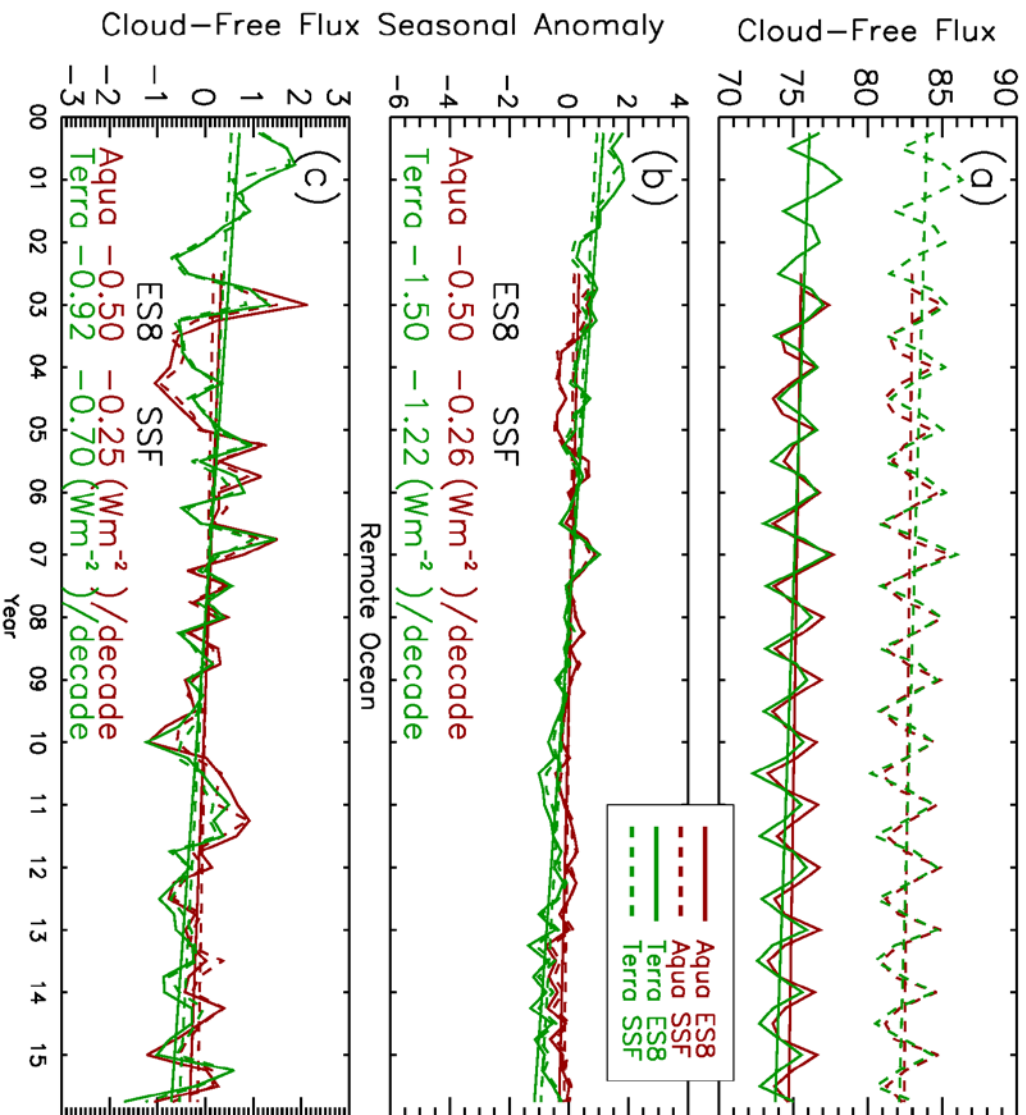
1071
 1072

1073
1074

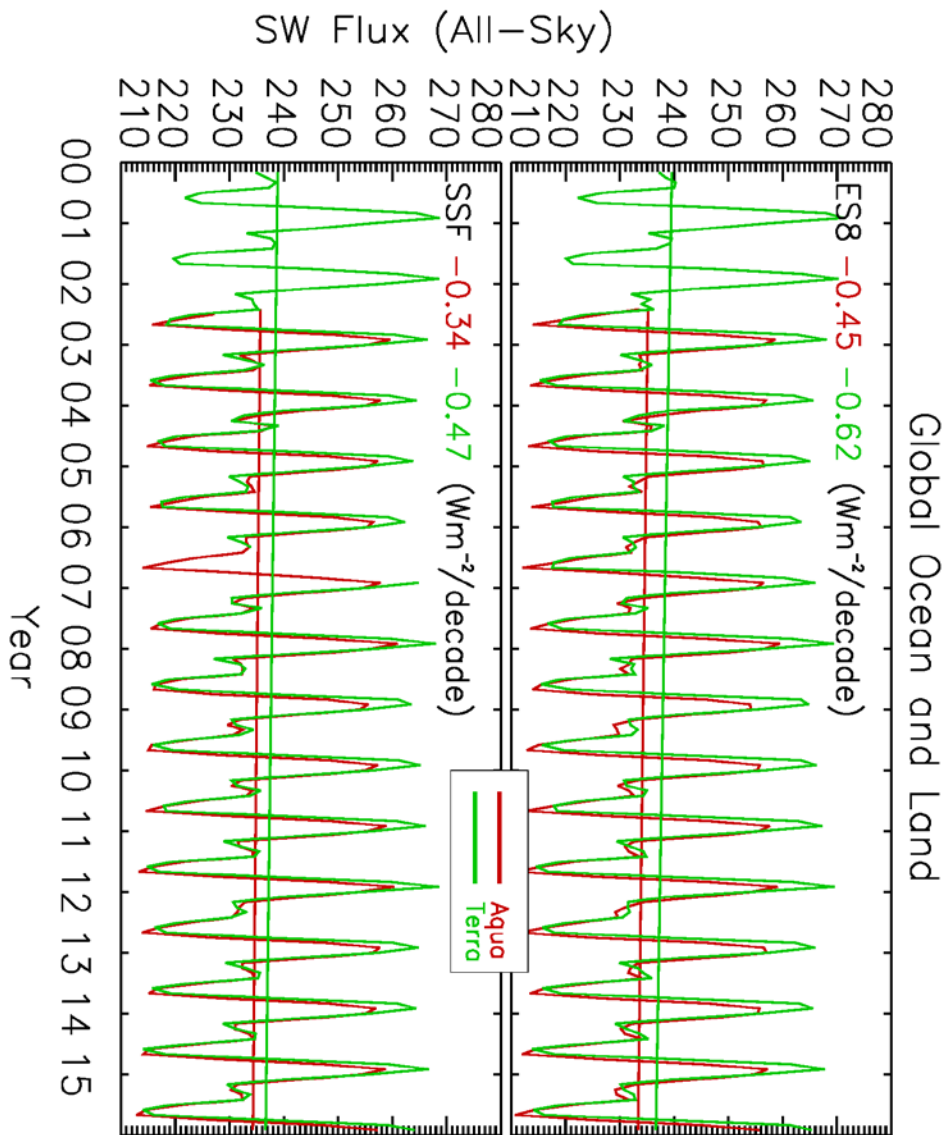


1075
1076
1077
1078
1079
1080
1081

Figure 7. Similar to Fig. 6, but for using collocated MODIS and CERES ES-8 cloud-free SW flux data.



1085 **Figure 8.** (a) Time series of seasonally-averaged, deseasonalized cloud-free SW fluxes over
 1086 global oceans utilizing the collocated MODIS-CERES (SSF/ES-8) datasets for Terra (green) and
 1087 Aqua (red). (b) Similar to Fig. 8a but using data from the Remote Ocean region. The ES-8 SW
 1088 fluxes are depicted by solid lines where SSF SW fluxes are depicted by dashed lines.
 1089



1091 **Figure 9.** Time series of all-sky SW flux over the entire globe (land and ocean). The trends are
1092 calculated from monthly-globally averaged all-sky SW fluxes derived from the CERES SSF /
1093 ES-8 data. SW fluxes from all scenes including cloudy, clean, land and ocean are taken into
1094 account when calculating the monthly averages, which are gridded into a similar resolution as
1095 the collocated MODIS-CERES dataset ($2 \times 2^\circ$).
1096

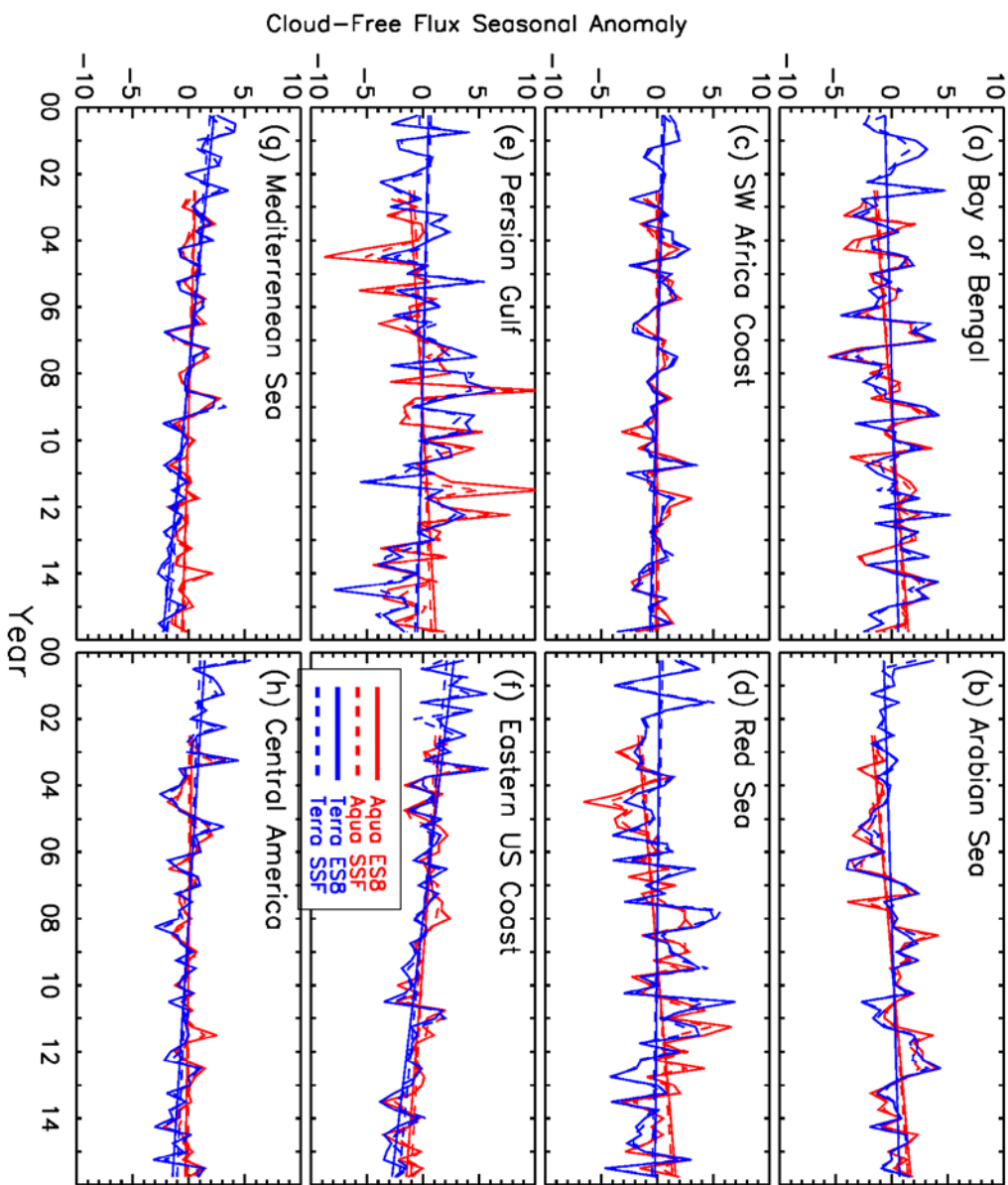
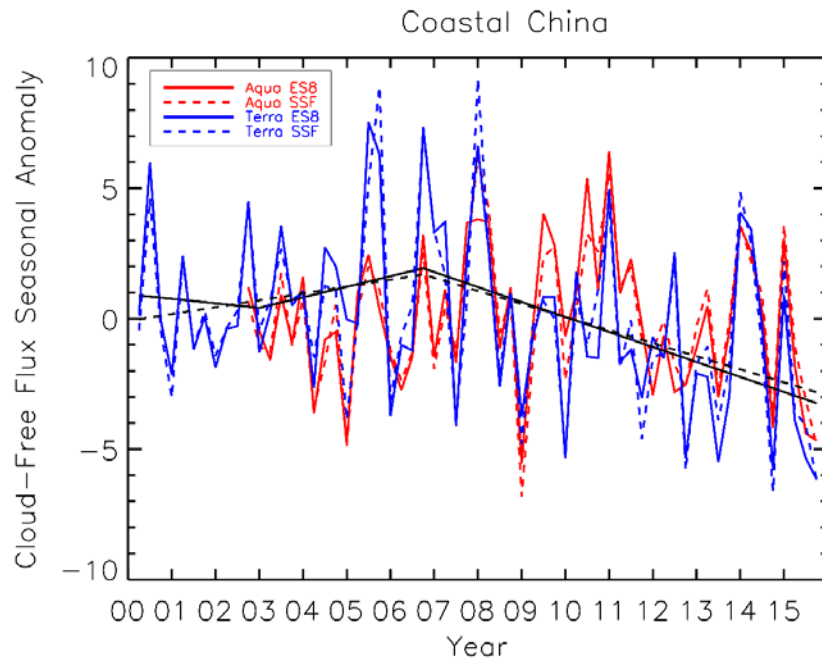
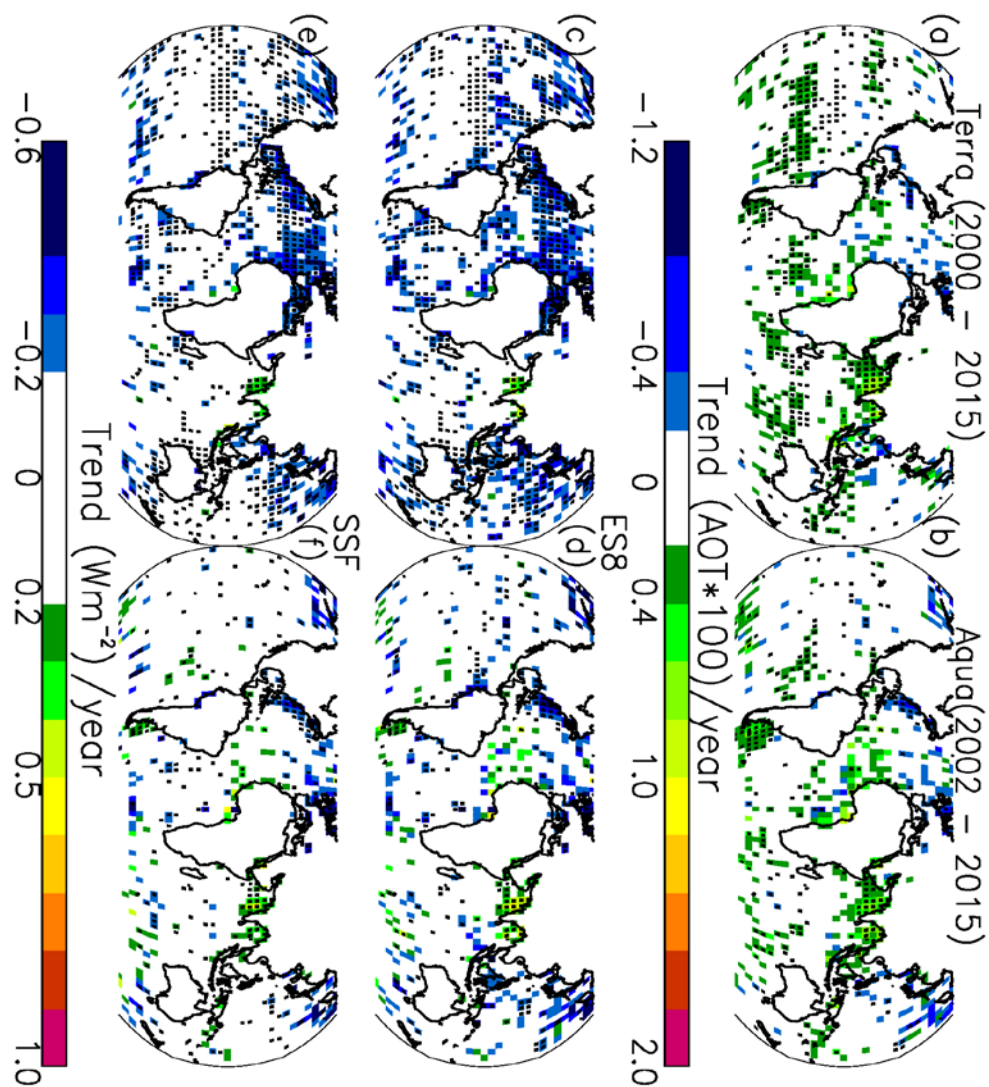


Figure 10. The temporal variations of deseasonalized, seasonally- and regionally- averaged CERES SSF / ES-8 cloud-free fluxes (seasonal anomaly) for 8 selected regions, constructed using the collocated Aqua and Terra MODIS-CERES datasets. The blue lines represent the Terra-based analysis while the red lines represent the Aqua-based analysis and the solid lines represent the ES-8 SW fluxes where the SSF SW fluxes are depicted by dashed lines.

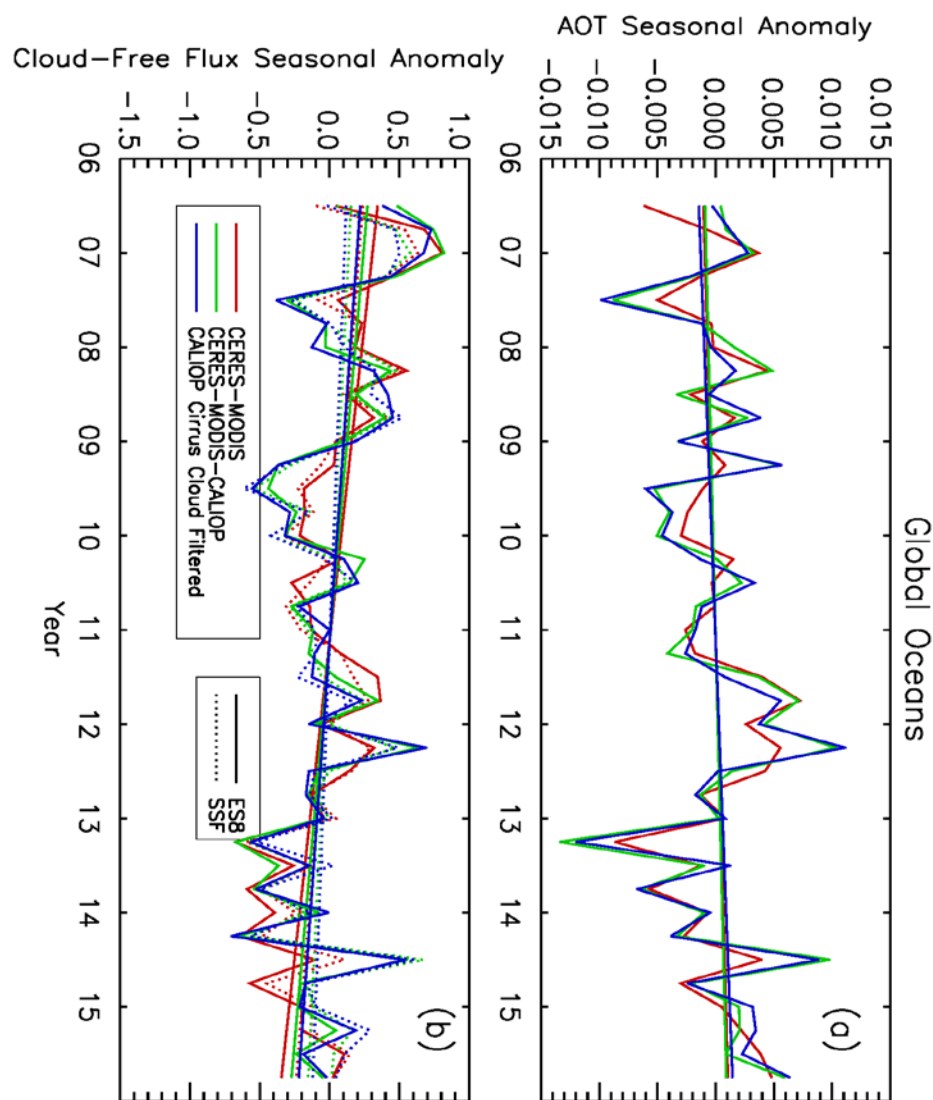


1103
 1104 **Figure 11.** The de-seasonalized, seasonally averaged cloud-free fluxes over the Coastal China
 1105 region derived utilizing the collocated MODIS-CERES (SSF / ES-8) datasets. Straight lines
 1106 show piecewise linear fits for the study periods of 2000–2008 and 2009–2015.



1107
 1108 **Figure 12.** Spatial distribution of gridded AOT trends for (a) 16 year Terra (2000-2015) and (b)
 1109 14 year Aqua (2002-2015) for every $4 \times 4^\circ$ (Latitude/Longitude) bin derived from the collocated
 1110 MODIS-CERES dataset. AOT trends are constructed using seasonally-averaged AOTs. (c)
 1111 Spatial distribution of cloud-free-sky CERES ES-8 SW flux trends estimated using the
 1112 collocated Terra MODIS-CERES data for the study period of 2000-2015. (d) Similar to Figure
 1113 12c, but using the collocated Aqua MODIS-CERES (ES-8) dataset for the study period of 2002-
 1114 2015. (e-f) Similar to Figs. 12c and 12d, but for using CERES SSF data. Grids with statistically

1115 significant AOT/clear-sky SW flux trends at the 95 % confidence interval are shown in black
 1116 dots.



1117
 1118 **Figure 13.** Global AOT trends derived from the (red) MODIS-CERES dataset, (green) MODIS-
 1119 CERES-CALIOP dataset and (blue) MODIS-CERES-CALIOP dataset after filtering for cirrus
 1120 clouds. Both CERES SSF and ES-8 data are included. Time series have been derived utilizing
 1121 seasonal AOT averages. CALIOP is used to locate and remove CERES observations

1122 contaminated with cirrus clouds. (b) Depicts the same thing as Fig. 13a, except for the cloud-free
1123 flux. This analysis is carried out for the Aqua-based study only.
1124